

# Fractal and Chaotic Dynamics in Nervous Systems

Chris C. King  
Department of Mathematics & Statistics,  
University of Auckland.

*Abstract : This paper presents a review of fractal and chaotic dynamics in nervous systems and the brain, exploring mathematical chaos and its relation to processes, from the neurosystems level down to the molecular level of the ion channel. It includes a discussion of parallel distributed processing models and their relation to chaos and overviews reasons why chaotic and fractal dynamics may be of functional utility in central nervous cognitive processes. Recent models of chaotic pattern discrimination and the chaotic electroencephalogram are considered. A novel hypothesis is proposed concerning chaotic dynamics and the interface with the quantum domain.*

## Contents :

0 : Introduction	2
1 : Concepts and Techniques in Chaos	2
(a) Chaotic Systems	2
(b) Indicators of Chaos	4
(i) Liapunov Exponent and Entropy	4
(ii) Power Spectrum	6
(iii) Hausdorff dimension and Fractals	7
(iv) Correlation Integral	8
(c) Iterations as Examples of Chaos	10
(i) The Logistic Map	10
(ii) The Transition from Quasiperiodicity to Chaos	14
(iv) Conservative systems and the Mixing Process	16
(d) Quasiperiodicity, Stochasticity and Chaos	17
(e) Chaos at the Quantum Level and Reduction of the Wave Packet	18
2 : The Modelling of Neural Systems	20
(a) Computational Processes and Causal Closure	20
(b) Mathematical Models of Neural Nets	22
(c) The Adaptive Resonance Architecture	23
(d) Comparison with Biological Nets	25
3 : The Diversity of Non-linear Characteristics of the Neuron and Synapse	26
(a) The Neuron	26
(b) The Synapse	29
4 : Evidence for Chaos and Fractal Dynamics in Excitable Cells	31
(a) Membrane Dynamics and the Chay-Rinzel Model	31
(b) Fractal Dynamics in a Voltage-dependent $K^+$ Channel	33
5 : Chaos and Chaotic Models in Neurosystems	35
(a) The Freeman-Skarda Model of the Olfactory Bulb	35
(b) Experimental Chaos in the Electroencephalogram	38
6 : The Fractal Extension of Chaos to the Quantum Level	42

## 0 : Introduction

This review surveys fractal and chaotic processes in brain dynamics and provides workers in experimental fields with a compact source of material in mathematical chaotic dynamics as a reference. An attempt has been made to make the mathematical aspects of the paper remain approachable to a variety of readers. Full background references are given to enable the reader to gain further in-depth treatment, and to explore more fully the variety of specialist topics leading out from the discussion.

Section 1 provides a compact mathematical introduction to fractal and chaotic dynamics. Most of the systems discussed here have specific application to experimental results in later sections. Sections 2 and 3 complement this with source material on mathematical modelling of neural nets and on biological neurons. In section 4 chaos at the cellular level is discussed, including models of the excitable membrane and ion channel. In section 5 chaotic neurosystems models and experimental results are considered including the Freeman-Skarda model and studies of the EEG. Section 6 touches on issues connecting quantum chaos, causality and the mind.

The aim of the review is to make it possible for a reader to gain a comprehensive overview of chaos as it applies to neural processes, to compare chaotic models with their alternatives and to assess the scope of chaotic and fractal processes in the conceptualization of the physical basis of brain function.

# 1: Concepts and Techniques in Chaos

(a) **Chaotic systems** This introduction provides a general description of chaotic dynamics and outlines techniques useful in analysis of experimental results.

A **dynamical system** is defined to be a set of first-order differential equations :

$$\dot{x}_i = \frac{dx_i}{dt} = F_i(\mathbf{x}, t) \quad i = 1, \dots, n \quad [1.1]$$

The system is called **autonomous** if  $F_i = F_i(\mathbf{x})$ , i.e. the functions are not changing with time.

Systems of higher-order differential equations can be reduced to first-order systems by a suitable change of variables. For example the equation of harmonic motion  $\ddot{x} = -x$  can be simply reduced to the system  $y = \dot{x}, x = -\dot{y}$ .

This type of formulation is general to Hamilton representations of conservative energetic systems, (see [2.2]).

A dynamical system is generally defined on a **configuration** space consisting of a **topological manifold**. A manifold is locally like Euclidean space  $\mathbb{R}^n$ , but may have varied global structures, as exemplified by the cylinder, torus, fig 5(a), Klein bottle and other higher-dimensional spaces.

Integration of the equations [1.1] to  $x_i(t) = I_i(\mathbf{x}(0), t) \quad i = 1, \dots, n \quad [1.2]$

yields **integral curves** or **trajectories** forming a flow on the manifold. The sets of these flow curves are called **orbits**. The flow thus integrates the field of velocity vectors determined by [1.1].

Linear differential equations admit analytic solutions and have well-defined asymptotic behavior as  $t \rightarrow \infty$ , converging to **fixed points**, or periodic oscillations, forming **closed orbits**. By contrast, even the simplest deviations from linearity, including quadratic, bilinear and piecewise-linear functions can, under suitable conditions, result in more complex **chaotic** behavior, in which the orbits of the system are attracted to a complex higher-dimensional subset called a **strange attractor**, or are **ergodic**. Ergodic flows behave like thermodynamic systems in that they can be modelled over statistical *ensembles* because the orbit fills a (possibly dense) set of invariant measure.

An **attractor** is a subset of the manifold to which an open subset of points, the **basin** of the attractor, tends in limit with increasing time. For example in fig 1(b) for  $v = +1$  the system has an attractor consisting of the closed circular orbit, with basins outlined by the arrowed flows. Existence of an attractor requires local volume to contract with increasing time and is consistent with a *dissipative* system in position-momentum representation. While *conservative* systems thus do not have attractors, they may still display classical chaos, see section 1(c)(iii).

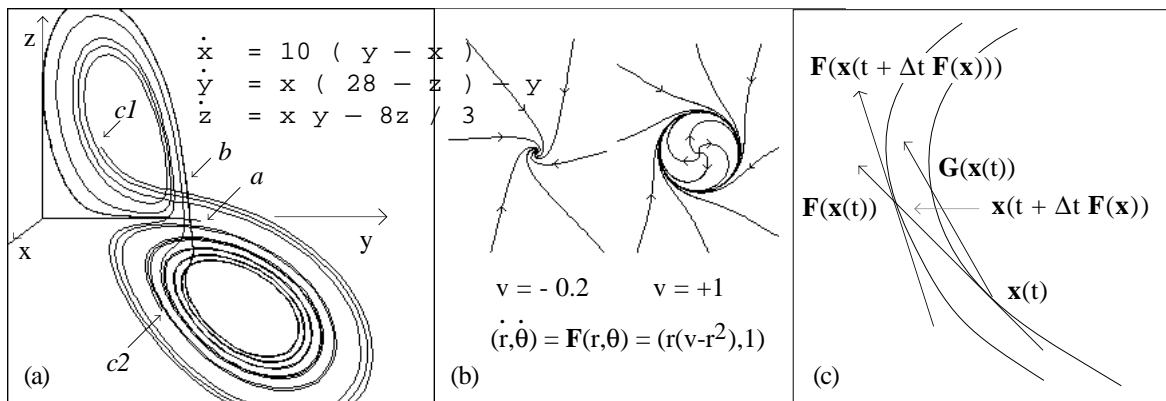


Fig 1 : (a) The Lorenz system displays sensitive dependence in which neighboring trajectories separate exponentially with time. Neighboring trajectories emanating from *a* are visibly separate by *b* and diverge into distinct spirals by *c1* and *c2*, so that their subsequent dynamics is unrelated.  
 (b) The Hopf bifurcation forms a periodic closed orbit attractor. For  $v < 0$  there is only a sink (attractor). As  $v$  crosses 0 an attracting periodic orbit and source (repellor) are created. The basins are indicated by the arrows.  
 (c) Geometric profile of the improved Euler method [1.4].

The hall-mark of a chaotic flow is **sensitive dependence on initial conditions** (Schuster 1986). Points which are arbitrarily close initially become exponentially further apart with increasing time, leading to the amplification of very small perturbations into global uncertainties. Sensitivity results in both an **entropy** increase associated with the loss of positional information with time, and in **structural instability** in which an arbitrarily small perturbation of the flow causes structural changes to the topology of the orbits ( although they may have similar qualitative behavior ). This prevents accurate long-term numerical approximation of the system with increasing time. In fig 1(a) sensitive dependence is illustrated. Neighboring trajectories emanating from *a* are visibly separate by *b* and diverge into distinct spirals by *c1* and *c2*, so that their subsequent dynamics is unrelated. Note that each orbit has a unique *winding sequence* e.g. 1, 6, 3, 4, ... representing the number of times it

negotiates each spiral arm of the attractor. An arbitrarily small perturbation will disrupt the winding sequence and hence change the topology of the orbits. The entropy results in a loss of memory of the initial conditions in any numerical approximation over time. The initial conditions thus cannot be retrieved by reverse iteration of the flow.

Time-dependent systems are capable of abrupt changes in their topological form called **bifurcations** as the underlying parameters cross critical values. Bifurcations result in abrupt *catastrophic* change in the topology of the flow under continuous variation of the time-dependent parameters. In fig 1(b) the *Hopf bifurcation* results in the formation of a closed orbit attractor (oscillation) from a point attractor (sink) at the origin as  $v$  crosses 0, see section 1(c)(ii). In fig 4(a) repeated *pitchfork bifurcations* result in subdivision of the logistic attractor, and the *tangent bifurcation* results in intermittent chaos, section 1(c)(i).

Because non-linear differential equations cannot in general be integrated directly, it is often necessary to resort to techniques of numerical integration in which a discrete **transfer function** is constructed which approximates a stroboscopic representation of the flow at discrete time intervals

$$\mathbf{x}(k\Delta t) = \mathbf{G}^k(\mathbf{x}(0)) \quad k = 1, 2, \dots \quad [1.3]$$

by using numerical methods such as the improved Euler method [1.4] or Runge-Kutta (Butcher 1987) :

$$\mathbf{x}_i(t + \Delta t) = \mathbf{G}_i(\mathbf{x}(t)) \approx \mathbf{x}_i(t) + \frac{\Delta t}{2} (\mathbf{F}_i(\mathbf{x}(t)) + \mathbf{F}_i(\mathbf{x}(t) + \Delta t \mathbf{F}(\mathbf{x}(t)))) \quad [1.4]$$

In a time-varying system, chaos may become established by three principal routes involving a (possibly infinite) sequence of bifurcations of the attractor, intermittent disruption of a periodicity, or the topological breakup of a surface, such as a torus, representing several linked oscillations. We will examine each of these three routes, because a knowledge of all of them is essential in characterizing chaotic dynamics in the brain and excitable cells.

**(b) Indicators of Chaos**

A series of techniques have been developed for analysing chaotic systems which both lead to a conceptual understanding of their phenomenology and also provide methods for handling experimental investigations. These are outlined in the following sections.

**(i) Liapunov Exponent and Entropy.** Two of the most important attributes of chaotic systems are sensitive dependence on initial conditions and the loss of spatial information with time, resulting in an entropy.

In a flow with sensitive dependence the distance between adjacent points becomes exponentially further apart with increasing time. Repeated iteration of the corresponding chaotic map similarly causes the separation of two adjacent points to become exponentially increased. This provides a means of calculating the exponent of growth, called the Liapunov exponent.

Consider the repeated action of the discrete map  $x_{n+1} = G(x_n)$  increasing separation by a factor  $a = e^{\lambda(x_0)}$ .

$$\begin{array}{ccc} \varepsilon & \xrightarrow{\quad} & \varepsilon e^{N\lambda(x_0)} \\ \left| \begin{array}{cc} x_0 & x_0 + \varepsilon \end{array} \right| & \xrightarrow{\quad G^N(x_0) \quad} & \left| \begin{array}{cc} G^N(x_0) & G^N(x_0 + \varepsilon) \end{array} \right| \end{array}$$

Hence we can write  $\varepsilon e^{N\lambda(x_0)} = \left| G^N(x_0 + \varepsilon) - G^N(x_0) \right|$ .

If the separation varies along the path, we can take limits as  $\varepsilon \rightarrow 0, N \rightarrow \infty$  we have

$$\lambda(x_0) = \lim_{N \rightarrow \infty} \lim_{\varepsilon \rightarrow 0} \frac{1}{N} \log \left| \frac{G^N(x_0 + \varepsilon) - G^N(x_0)}{\varepsilon} \right| = \lim_{N \rightarrow \infty} \frac{1}{N} \log \left| \frac{d G^N(x_0)}{d x_0} \right| \quad [1.5]$$

$$= \lim_{N \rightarrow \infty} \frac{1}{N} \log \left| \frac{d G(\dots G(x_0) \dots)}{d x_0} \right| = \lim_{N \rightarrow \infty} \frac{1}{N} \log \left| \prod_{i=0}^{N-1} G'(x_i) \right| = \lim_{N \rightarrow \infty} \frac{1}{N} \sum_{i=0}^{N-1} \log | G'(x_i) | \quad [1.6]$$

This formula makes it easy to calculate the Liapunov exponent for any iteration. In a chaotic system in one or more variables, sensitive dependence requires at least one of the Liapunov exponents to be greater than 1, thus resulting in exponential separation of trajectories.

Note that in the case of a continuous flow, the role of the constant  $a$  is slightly different.

In the flow

$$\dot{\mathbf{x}} = \mathbf{a}\mathbf{x} \rightarrow \mathbf{x}(t) = e^{at} \mathbf{x}(0),$$

[1.7a] whereas with the map,

$$x_{n+1} = e^a x_n \rightarrow x_n = e^{an} x_0. \quad [1.7b]$$

The formula [1.6] also naturally represents the loss of information, or entropy :

The Shannon informational entropy is 
$$I_1 = - \sum_{i=1}^n P_i \log_2 P_i \tag{1.8}$$

where  $P_i$  is the probability of being in state  $i$  and  $\log_2 = \log_2$ .

Consider a single iteration in which  $[0,1]$  maps to  $[0,1]$  under separation  $a$ . At the initial stage, we have  $n$  states

each with probability  $\frac{1}{n}$ , so : 
$$I_{in} = - \sum_{i=1}^n \frac{1}{n} \log_2 \frac{1}{n} = \log_2 n \tag{1.9}$$

After one iteration, the resolution is reduced by factor  $a = |G'(o)|$ , following the same reasoning as in [1.6] for one step, giving  $\frac{n}{a}$  states each with probability  $\frac{a}{n}$ ,

so we have : 
$$I_{fin} = - \sum_{i=1}^{n/a} \frac{a}{n} \log_2 \frac{a}{n} = \log_2 \frac{n}{a} \tag{1.10}$$

Thus there is thus a difference 
$$\Delta I = I_{in} - I_{fin} = \log_2 a = \log_2 |G'(o)|.$$

Averaging this over many iterations, we have 
$$\overline{\Delta I} = \lim_{N \rightarrow \infty} \frac{1}{N} \sum_{i=0}^{N-1} \log_2 |G'(x_i)| \tag{1.11}$$

which is obviously the same as [1.6] except for a factor of  $\log_2$ .

For a 1-dimensional map we thus define the **Kolmogorov entropy** to be  $K = \lambda$ .

When we have a higher-dimensional mapping or flow, there is an exponent  $\lambda_i$  for each dimension  $i$  in the configuration space. If the system has an attracting set, volume contraction will cause the sum of the exponents to be negative, thus allowing only some to be positive. Only the positive (expanding) Liapunov exponents contribute to the spreading and so  $K$  is generally identified with the sum of these positive exponents.

$$K = \sum_{\lambda_i > 0} \lambda_i \tag{1.12}$$

A system with more than one positive exponent is referred to as *hyperchaotic* (Rössler 1979,1988).

From another point of view, the entropy may be associated with *new* information entering the system and over time replacing that associated with the initial conditions.

**(ii) Power Spectrum.** To distinguish between chaotic and multiply periodic systems one can examine the

**Fourier transform** 
$$x(\omega) = \lim_{T \rightarrow \infty} \int_0^T e^{i\omega t} x(t) dt \tag{1.13}$$

which transforms the function  $x(t)$  into a spectrum  $x(\omega)$  of frequency components, which for periodic motion consists of discrete frequencies, but for chaotic motion has a broad band spread.

The **power spectrum** squares the Fourier amplitudes to give positive real values

$$P(\omega) = |x(\omega)|^2 \tag{1.14}$$

In the case of a discrete iteration of finite length, such as a  $2^n$  cycle, we can use a discrete transform to resolve the

iteration into its Fourier components 
$$x^n(t) = \sum_k a_k^n e^{2\pi i k t / 2^n} \tag{1.15}$$

This results for example in the 1024 step and 256 step Fast Fourier Transforms [FFTs] shown in fig 2(a). In (i) a 1024 point iteration of one component of the Lorentz iteration has been used to generate the discrete power spectrum using a Fast Fourier Transform [FFT] (Elliot et. al.. 1982). Although the flow has a strong periodicity its band-spread indicates chaos. (ii) The FFT of the self-similar Morse-Thule sequence (Schroeder 1986) 0110100101101001. . . This can be generated by recursive reflection of 01 in its complement [viz 01, 0110, 01101001, etc.], or by taking the binary digit sums of each positive integer mod 2, [viz  $0 \rightarrow 0, 1 \rightarrow 1, 10 \rightarrow 1, 11 \rightarrow 0$  etc.]. Although this is non-repeating, any discrete Fourier transform has a symmetric set of distinct components, as a result of symmetries in the self-similar structure.

**(iii) Hausdorff Dimension and Fractals.** In a one-dimensional set such as the interval  $[0,1]$ , we need twice as many subsets of  $1/2$  the length to cover the interval, 4 times as many of a  $1/4$  the length and so on. In a two dimensional set, such as the unit square, we need  $2^2$  times as many  $1/2$  the length and so on. We can thus define the

**Hausdorff dimension**  $d$  as the exponent such that a covering by  $d$ -spheres of diameter  $\epsilon$  satisfies 
$$N(\epsilon) \propto \epsilon^{-d}, \text{ as } \epsilon \rightarrow 0. \tag{1.16}$$

A set is called a **fractal** if its Hausdorff dimension exceeds its integral topological dimension, i.e. if the Hausdorff dimension is not an integer.

Fractals often possess *self-similarity* on a change of scale between parts of the set and the whole. A fractal which is constructed by recursive development in stages, enables exact calculation of the Hausdorff dimension from [1.16] using two successive stages of length  $\epsilon$  and  $\epsilon'$ :

$$d_f = - \frac{\log [ N(\epsilon) / N(\epsilon') ]}{\log [\epsilon / \epsilon']} \quad [1.17]$$

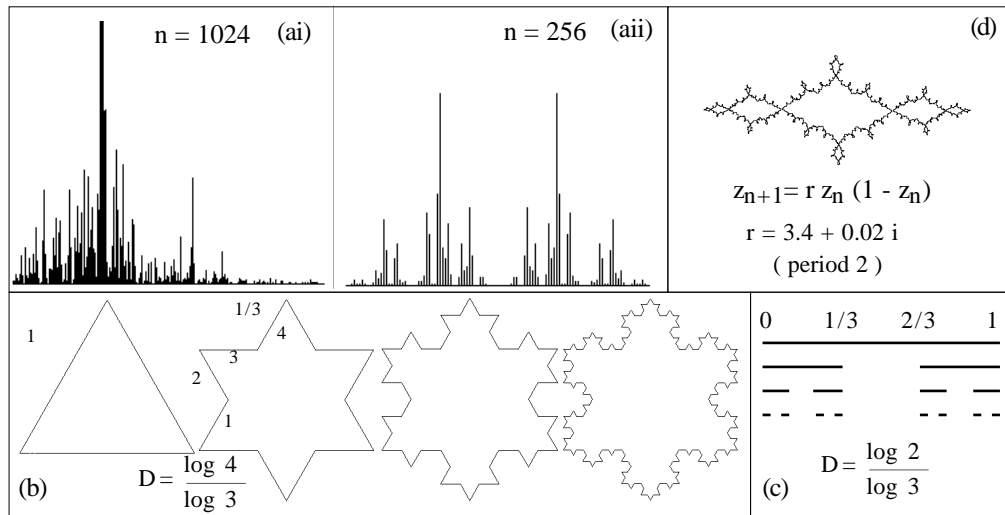


Fig 2 : (a) Power spectra (i) for the Lorentz system and (ii) for the Morse-Thule sequence. Note the broad bandspread in (i) characteristic of chaos despite the existence of a peak frequency. In (ii) although the sequence is self-similar and non-periodic, the power spectrum consists of symmetrical frequencies. (b) Koch flake formed by repeated tessellation of a triangle and (c) Cantor set formed by repeated removal of the central third of each interval are examples of fractals. (d) Julia set of complex logistic map [1.24] for  $r = (3.4 + .02 i)$ . This set is connected so that points near zero iterate to a finite period attractor inside the set. Points outside all iterate to infinity. Julia sets can also be disconnected, in which case all other points iterate to infinity.

For example in the Koch flake, fig 2(b) each side is repeatedly replaced by 4 sides each  $\frac{1}{3}$  the length. This gives rise to a Hausdorff dimension of  $\frac{\log 4}{\log 3} = 1.26$  in the limit, hence a fractal. The Cantor set, fig 2(c) is formed from  $[0,1]$  by removing the open middle third [e.g.  $(\frac{1}{3}, \frac{2}{3})$ ] from each remaining subinterval, leaving 2 sides of  $\frac{1}{3}$  the length.

It is thus a fractal with dimension  $\frac{\log 2}{\log 3} = 0.63$ . Note that the Cantor set is identifiable with all base 3 numbers in  $[0,1]$  having only 0 & 2 as digits, e.g. 0.0220020... and thus maps 1-1 onto the whole interval  $[0,1]$  by mapping e.g. 0.0220020  $\rightarrow$  0.0110010. This occurs despite the removal of a set of measure

$$\sum_{n=0}^{\infty} \frac{1}{3} \left(\frac{2}{3}\right)^n = \frac{1/3}{1 - 2/3} = 1, \text{ equal to that of the whole interval } [0,1]!$$

The strange attractors of chaotic dynamics are generally fractals. A finite non-integer dimension indicates that a dynamic is chaotic, rather than stochastic. Iterations such as the logistic map [1.23] result in fractals called **Julia sets** fig 2(d), subsets which tend neither to a finite attractor nor to infinity, but are mapped within themselves. They thus form the *fractal boundaries* of the basins of attraction. The variety of Julia sets of the quadratic mapping  $z_{n+1} = z_n^2 + r$  has been the subject of keen interest (Peitgen & Richter 1986), as well as their relation to the Mandelbrot set fig 4(a). The Julia set of each value  $r$  is a unique self-similar fractal each with its own distinctive form. Given a connected Julia set, such as the one illustrated in fig 2(d), for the period 2 region of the logistic map, points on the interior basins all iterate to a finite attracting set, while those outside iterate to infinity. The bounding Julia set consists of those chaotic points which do neither. Such fractal basin boundaries appear to be general in dynamical systems. Time-dependent systems may also generate fractal spatial bifurcations to form **dissipative structures** enabling the generation of fractal order out of chaos.

(iv) **Correlation Integral.** We can generalize the fractal dimension as follows (Grassberger & Procaccia 1983, Roschke & Basar 1989). Consider a covering, as above, with spheres of radius  $\varepsilon$ ,  $P_i$  the probability that a point falls into sphere  $i$ , and  $N(\varepsilon)$  the number of non-empty spheres. Then we define the Rényi information of order  $q$  as :

$$I_q(\varepsilon) = \frac{1}{1-q} \log \sum_{i=1}^{N(\varepsilon)} P_i^q, \quad q \neq 1 \quad \text{and} \quad I_1(\varepsilon) = - \sum_{i=1}^{N(\varepsilon)} P_i \log P_i \quad [1.18]$$

and the dimension 
$$d_q = \lim_{\varepsilon \rightarrow 0} \frac{I_q(\varepsilon)}{\log [1/\varepsilon]} \quad [1.19]$$

Thus  $d_0 = \lim_{\varepsilon \rightarrow 0} \frac{\log N(\varepsilon)}{\log [1/\varepsilon]} \propto d_f$  above;  $d_1$  &  $d_2$  are called the **information & correlation** dimensions. Grassberger & Procaccia (1983) formulated the correlation dimension into a useful algorithm as follows:

$$I_2(\varepsilon) = - \log \sum_{i=1}^{N(\varepsilon)} P_i^2 = - \log C(\varepsilon) \quad [1.20]$$

where  $C(\varepsilon)$  is the probability of points having distance  $|x_i - x_j| < \varepsilon$ , since each  $P_i^2$  is the probability of  $x_i, x_j$  being in the same  $\varepsilon$ -sphere.  $C(\varepsilon)$  can be calculated explicitly using the Heaviside step function.

$$C(\varepsilon) = \lim_{n \rightarrow \infty} \frac{1}{n^2} \sum_{i,j=1}^n \Theta(\varepsilon - |x_i - x_j|), \quad \Theta = \begin{cases} 1, & x > 0 \\ 0, & x < 0 \end{cases} \quad [1.21]$$

Since 
$$d_2 = \lim_{\varepsilon \rightarrow 0} \frac{\log C(\varepsilon)}{\log \varepsilon}, \quad \text{we have } C(\varepsilon) \propto \varepsilon^{d_2} \quad [1.22]$$

making it possible to do a plot of  $\log C(\varepsilon)$  against  $\log \varepsilon$ , to test for linearity, fig 3(c).

The correlation dimension is thus a more accessible measure of the dimension of a chaotic attractor than the fractal dimension, which is more difficult to calculate from a trajectory partly because the points do not become evenly spread on the attractor. Dimensions vary from 2.06 for the Lorenz attractor, through 4 for e.e.g. recordings of epileptic states through to values around 9 for a stochastic process with a small degree of correlation between the sample variables.

Because a long time series of vectors  $\mathbf{x}_1, \dots, \mathbf{x}_n$  in the dynamic will have most of its variables uncorrelated because of exponential divergence of the trajectories, correlations between the variables will be a consequence of their lying on the attractor. Modifications of the Grassberger-Procaccia algorithm have been proposed (Theiler 1987, Albano et. al. 1988, Rapp et. al. 1989) which improve both speed and accuracy.

As a result of Taken's (1981) proof, a 1-D time series can be used to form an *embedding space* for the attractor by taking  $\kappa$ -vectors  $x_{i\tau}, x_{(i+1)\tau}, \dots, x_{(i+\kappa-1)\tau}$ , by taking a suitably large value for the dimension  $\kappa$ . Increasing the time delay  $\tau$  results in a saturation level  $\tau_{\text{sat}}$  for a given  $\kappa$  as the sampling time becomes long enough to ensure non-correlation, fig 3(a). As  $\kappa$  is increased,  $\tau_{\text{sat}}$  increases to a plateau, thus determining suitable  $\kappa, \tau$  and hence  $d_2$  (Roschke & Basar 1989), fig 3(b). Various problems still remain. A suitable choice of the window length  $(\kappa-1)\tau$  and of the overall time epoch of the sample must be made. A good measurement of  $d_2$  is made only if the slope of the *log-log* plot remains say within a 10% variation over at least an adjustment of a factor of 2 in  $\varepsilon$  (Rapp et. al. 1989). A plot of the slope against  $\log \varepsilon$  is useful here. The upper and lower bounds defining the region should be indicated. One reasonable indicator of window length is to use the autocorrelation function

$$g(t) = \frac{\sum_i x_{i\tau} x_{i\tau+t}}{\sum_i x_{i\tau}^2} \quad [1.23]$$

to define the *correlation time* when the autocorrelation function has fallen from 1 at  $t=0$  to  $1/e$  (Albano et.al. 1988).

A good plateau in the slope depends on a suitable window length a few times larger than the correlation time. Too short a window fails to provide a good plateau, on the other hand, making the window too large can result in the values no longer strictly adhering to a single trajectory and violating Taken's embedding theorem. Similarly care had to be taken with the time-epoch, which should be as long as possible but not long enough to result in non-stationarity in the phenomenon being measured. Researchers devising experimental tests for chaos are advised to consult Rapp (1989) before choosing their design and protocol. See also section 1(d).

It is also possible to measure the correlation dimension by taking a series of measurements from distinct spatial points in the dynamic, however this may result in a lowering of the measured value because the presentation of the attractor from the spatial sample is not fully unfolded (Babloyantz 1989).

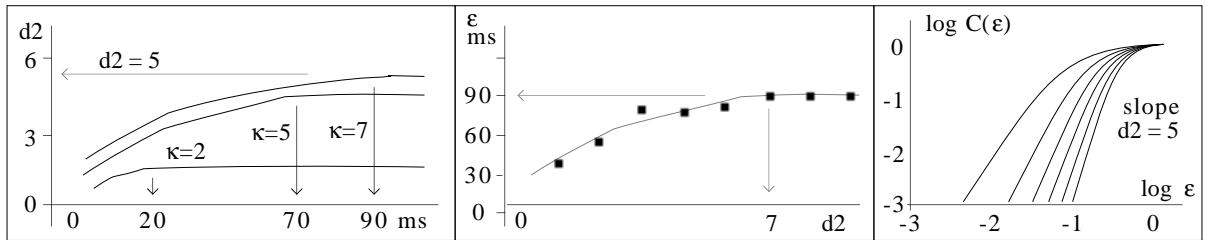


Fig 3 : The experimental determination of correlation dimensions requires testing of parameters for saturation. (a)  $\tau_{\text{sat}}$  versus  $\kappa$ , as different embedding dimensions are used and the delay  $\kappa$  is increased, saturation occurs in the estimated dimension for different delays. Adequate delay must be provided in each embedding dimension to get a correct figure. (b) plateau in  $\tau_{\text{sat}}$  at  $\kappa = 7$ , illustrates that adequate embedding dimension is also essential. (c)  $d_2$  from slopes of  $\log C(\epsilon)$ - $\log \epsilon$  plots has limit at  $\kappa = 7$ . The dimensions are actually calculated from the limiting slope of  $\log C(\epsilon)$  against  $\log \epsilon$ . Checks should be made both that the parameters used do give linearity in the parameter range and that they do converge to a good limit value.

### (c) Iterations as Examples of Chaos

(i) **The Logistic Map.** Chaotic dynamics occur in some of the simplest iterative functions, including piecewise-linear and quadratic functions. To develop several aspects of chaotic behavior, we will examine a typical quadratic iteration, the logistic map :

$$x_{n+1} = G_r(x_n) = r x_n (1 - x_n) \quad [1.24]$$

representing exponential population growth subject to a constrained area (Schuster 1986, Devaney & Keen 1989). The term  $r x_n$  determines of exponential growth while the additional term  $(1 - x_n)$  places a finite area constraint limiting the population.

It is easy to picture such an iteration in various ways. One is to successively evaluate the functions  $y = r x (1 - x)$  and  $x = y$  as shown in fig 4(b<sub>i</sub>). We pick an initial value  $x$  and evaluate  $y$  by moving vertically to the parabola. Next we let  $x = y$  by moving horizontally to the sloping line. The two steps combined result in one iteration i.e.  $x_{n+1} = y = r x_n (1 - x_n)$ .

As the parameter  $r$  varies, the behavior of the iteration goes through a sequence of different stages. In (b<sub>i</sub>) the iterations are illustrated for  $r = 1$  and 2 starting from two arbitrary points in  $[0,1]$ . Each iterates toward a fixed point, one at zero and the other positive. For the remaining figures the iteration is left to run for a few hundred steps, before plotting, so that only the limiting attractor is highlighted. Near the value 3.4 the iteration is attracted to a set of two values i.e. period 2, as depicted in (b<sub>ii</sub>), in which the arrows still indicate the  $y = r x (1 - x)$  and  $x = y$  steps. At 3.56, (b<sub>iii</sub>), the period 2 orbit has bifurcated twice to form a period 8 orbit. The effect of such period doubling is clearly seen in the braided form of the attractor path. At 3.66, (b<sub>iv</sub>), chaos has set in and the orbits now spread irregularly across the interval without returning exactly. At 3.8282 (b<sub>v</sub>) we are very close to the period 3 window. The period 3 iteration keeps slipping however, and intermittently enters chaos before returning to the attractor. At 3.8289 (b<sub>vi</sub>) period 3 has become stable. At 4.5 (c) the attractor has broken up and now most points escape to  $-\infty$ . A residual Cantor set of points (the Julia set) is mapped amongst itself, forming a Smale horseshoe (see section 1(c)(iii)).

Alternatively, we can plot all the  $x$  values that occur for a given  $r$ , once the system has been allowed to approach the attractor, as shown in fig 4(a). This gives rise to the *attractor form* diagram in which an initial point attractor repeatedly bifurcates into 2, 4, 8, ... values limiting in chaos at  $r_{\infty}$ , punctuated by further windows e.g. of period 3, and finally breakup of the attractor at  $r = 4$ .

Corresponding values of the *Liapunov exponent* are shown below this. For  $r < r_{\infty}$ ,  $\lambda \leq 0$ , reaching zero at each bifurcation point  $r_i$ , but once chaos begins,  $\lambda > 0$ , except for brief negative dips in the periodic windows.

The sector of the *Mandelbrot set* of the logistic map fig 4(a) illustrates the fractal nature of the envelope of iterates when both  $x$  and  $r$  have complex number values. These enable us to visualize the fractal structures more easily because they form a plane. Each  $r$  value in the Mandelbrot set gives rise to a connected Julia set fig 2(d) and will hence iterate the central value  $x = 1/2$  to a finite attractor separated from infinity by the connected Julia set (e.g. *inside* the Julia set of fig 2(d)). The complement of the Mandelbrot set will iterate  $1/2$  to infinity. In fig 4(a) the Mandelbrot set becomes vertically extensive only for  $r$  values whose real part has Liapunov exponent  $\lambda < 0$ . For  $\lambda \geq 0$  it is confined to the real line, extending a thread to the value 4 with tiny islands showing for  $r$  values in the odd period windows. The Mandelbrot set, and particularly its complement near their boundary, is famous for the beauty of its color contour computer iterations. It has been described as the most complex object in mathematics.

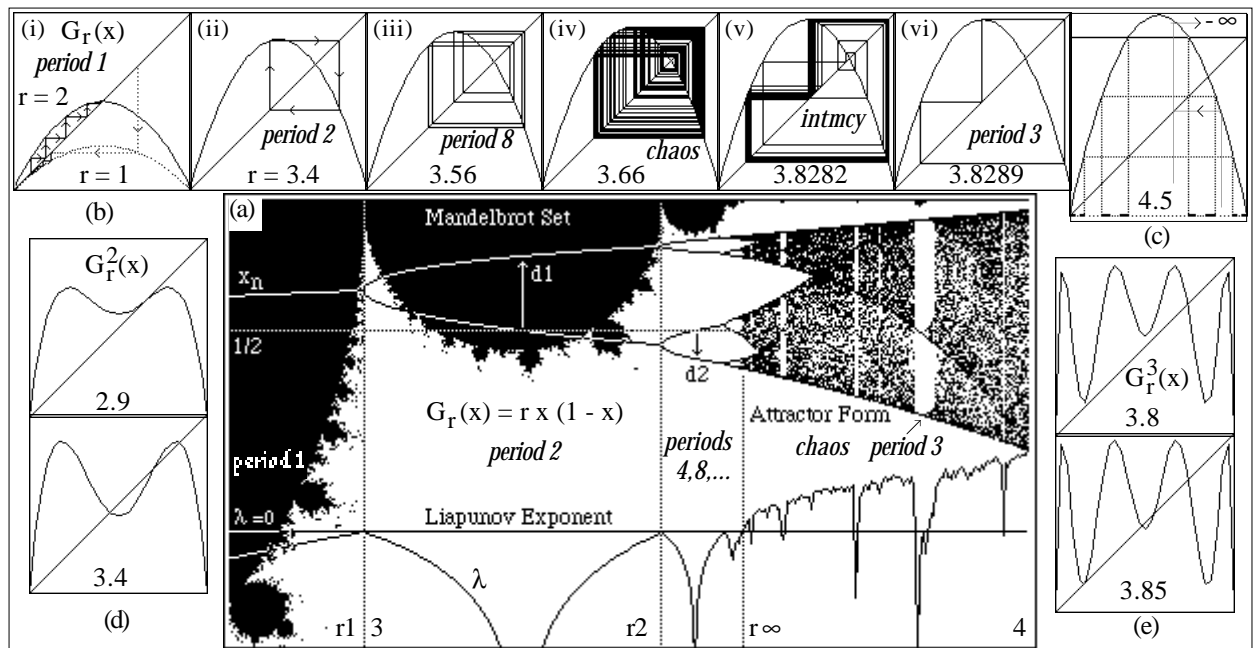


Fig 4 : The logistic map : The text contains a complete description of all the phenomena in the diagram.

(a) The forms of the attractor, Liapunov exponent and Mandelbrot set, for  $2.8 \leq r \leq 4$  showing the development of multiple period doublings, chaotic regions and periodic windows. The attractor initially is a single curve (point attractor) but then repeatedly subdivides (pitchfork bifurcations) finally entering chaos (stippled band). Subsequently there are windows of period 3, 5 etc. with abrupt transitions from and to chaos caused by intermittency and crises. The Liapunov exponent  $\lambda \leq 0$  until chaos sets in. During chaos it remains positive. The Mandelbrot set illustrates the fractal nature of the periodic and chaotic regimes when  $x$  &  $r$  are extended to the complex number plane.

Complex number representation aids visualizing such fractal structures.

(b) A series of 2-D iterations of  $G_r(x_n)$  including periods 1, 2 and 8 chaos, intermittency, and period 3. In (i) the two-step iteration process is illustrated alternately evaluating  $y = r x (1 - x)$  (vertical) and  $x = y$  (horizontal). As  $r$  crosses the value 1 a saddle-node bifurcation occurs resulting in the attractor moving from zero and leaving a repeller there ( $r = 2$ ). In (ii) & (iii) period 2 and 8 attractors have formed. In (iv) the iteration has become chaotic.

In (v) the chaos is intermittently entering a period 3 regime, which has become stable in (vi).

(c) The Cantor set of the horseshoe for  $r = 4.5$ . The attractor has now broken up resulting in most points iterating to minus infinity, leaving only a Julia set of exceptional points. (d) The pitchfork bifurcation illustrated. The double iterate  $G_r^2(x_n)$  twists to cross  $y = x$  an extra time, resulting in doubling of the attractor into a period 2 set.

(e) The tangent bifurcation illustrated using the triple iterate  $G_r^3(x_n)$ . The lifting of the central tangent above  $y = x$  removes the stability of period 3 causing slippage and intermittent chaos.

We will examine the variety of dynamical phenomena which occur in the Logistic map by looking qualitatively at six situations, each of which highlights a distinct feature of importance :

(1) **Point attractors** : When  $r = 0$  the attractor is initially zero. As the parameter  $r$  is increased from 0, the quadratic rises and at 1 crosses the line  $y = x$  resulting in a **saddle-node** bifurcation in which a single attractor becomes a pair : an attractor and a repeller. In higher dimensional situations we would have a saddle, fig 6(c) and an attractor or repeller (node). The point attractor moves up to positive  $x$ , leaving a repeller at 0. Outside  $[0,1]$  the iteration tends to  $-\infty$ . This situation is illustrated in fig 4(b<sub>i</sub>) where for the transitional value  $r = 1$  the iteration is still attracted down and to the left to zero, while for  $r = 2$ , zero is a *repeller* and the intersection of the parabola with the line  $y = x$  is an *attractor*.

(2) **Period doubling** : At value  $r_1 \sim 3$  there is a bifurcation of the fixed attractor into a period 2 attracting set, as illustrated in (b<sub>ii</sub>). Successive period doublings at  $r_2$  etc., (b<sub>ii</sub>, iii) cause the attractor to have a sequence of periods 2, 4, 8, ...,  $2^n$ . These arise from **pitchfork bifurcations** as illustrated obviously in the forkings of attractor form in (a). Here the graph of the two-step iterate  $G_r^2(x) = G_r(G_r(x))$  twists across  $y = x$  to cause a doubling of the period. In this range the Liapunov exponent  $\lambda < 0$ , except at  $r_1, r_2$ , etc. where  $\lambda = 0$ .

**Universality** : In (a) are outlined the bifurcation values  $r_1, r_2, \dots, r_\infty$  and the distances  $d_1, d_2, \dots$

where  $d_n$  are the widths of the period  $2^n$  attractors where they straddle the symmetrical value  $1/2$ .

$$\text{The values} \quad r_n = r_\infty - C \delta^{-n} \quad \& \quad d_n = \frac{d_{n-1}}{-\alpha} \quad [1.25]$$

are determined by the **Feigenbaum numbers**  $\delta = 4.669$ , and  $\alpha = 2.502$ . These are universal to all functions with a quadratic maximum and thus appear in a variety of systems from biology to astronomy (Stewart 1989).

(3) **Chaos** : At the limit value  $r_\infty$  the iteration becomes chaotic, ( $b_{iv}$ ) and  $\lambda > 0$ . The trajectories now spread over the interval  $[0,1]$ . They do not recur as there are no finite periodicities, but approach each possible value arbitrarily closely given sufficient time. The iteration now has sensitive dependence,  $\epsilon$ -close initial points becoming exponentially separated. Although the orbits appear equally spread across the entire possible range of values, the details of each are structurally unique. Complexity grammars (Auerbach & Procaccia (1990) further analysis.

(4) **Odd Period Windows : Intermittency and Crises** There are a series of windows in the chaotic region where chaotic behavior is abruptly interrupted by new periodic regimes of periods 3, 5, etc., ( $b_{vi}$ ). These windows contain for example  $3.2^n$  bifurcation sequences similar to that of (2). As a result of Li & Yorke (1975), the existence of a period 3 attractor guarantees the existence of periods of all orders and uncountably many aperiodic orbits (chaos). By Sarkovski, the periods follow the causal sequence :

$$3 \rightarrow 5 \rightarrow 7 \dots 2^n.3 \rightarrow 2^n.5 \rightarrow \dots 2^4 \rightarrow 2^3 \rightarrow 2^2 \rightarrow 2 \rightarrow 1 \quad n = 1, 2, 3, \dots$$

At the left-hand end of the period 3 window, a new type of bifurcation, the **tangent bifurcation** occurs, in which the 3-cycle becomes intermittently disrupted by chaotic bursts, ( $b_v$ ). Intermittent disruption of a periodic dynamic constitutes a second route to chaos distinct from period doubling in which only a single bifurcation is required for chaos. These constitute two of the three classical route to chaos. In fig 4(e) the source of the tangent bifurcation is illustrated. The tangent to  $G_r^3(x)$  crosses  $y = x$  as  $r$  is decreased allowing the escape of the period 3 iteration. Immediately upon bifurcation, the tangent (upper fig) is adjacent to  $y = x$  causing a slow slippage of the 3-cycle with irregular breakout into short episodes of chaos. Hence the term **intermittency**.

At the right-hand end of the period 3 window is another type of abrupt transition to chaos called a **crisis** that is caused by a collision between a point repeller and the fanning chaotic sub-bands of period 3 forming small triangles in fig 4(a). This causes the chaos to be repelled so that it spreads suddenly across all values again. The 3 repellers originate from the birth of period 3 in the tangent bifurcation at the other end of the window.

(5) **Julia sets and Horseshoes** : For each value of  $r$  there is a residual fractal Julia set of exceptional points which do not converge to the attractors, but are mapped instead among themselves. The Julia set for an  $r$  value of the complex logistic map in the period 2 region is illustrated in fig 2(d). Complex values assist the visualization of Julia sets because complex numbers form a planar image which we can see.

For  $r > 4$  the finite attractor ceases to exist, since the graph now goes outside the unit square, allowing points to iterate to  $-\infty$ , however a Cantor set of points remains, fig 4(c) which are mapped among themselves indefinitely, once all the points which escape to  $-\infty$  in one or more stages are removed. These form a Smale horseshoe as described below, fig 6(b). This is in fact the Julia set of the mapping, which in this case is not a connected set, because of the destruction of the finite attractor's basin.

(6) **External noise** : In the presence of external noise, the higher periods become lost, leaving noisy low periods and chaos. Noise thus can mask high period attractors and create the impression of chaos, see fig 7.

(ii) **The Transition from Quasiperiodicity to Chaos**. A third route to chaos arises from the development of multiple ( in particular three ) frequencies through repeated Hopf bifurcations as illustrated in fig 5(a).

The Hopf bifurcation creates an oscillation by the formation of a cyclic closed orbit as in fig 1(b). Here the vector field  $\mathbf{F}$  expressed in terms of polar coordinates  $(r, \theta)$  has a constant rate of rotation, and a quadratic radial component dependent on  $v$ . For  $v < 0$  the radial component is negative for all  $r$  and hence the origin is a sink (attractor). As  $v$  crosses 0 a positive radial component develops. An attracting periodic closed orbit attractor (oscillation) is created, leaving a source (repeller) at the origin, as represented in 1(b) for the value  $v = 1$ .

The quasiperiodicity route is common in the development of turbulent phenomena through oscillations. The first and second Hopf bifurcations introduce two frequencies which can be realized as a flow on a 2-torus to which the rest of the flow is attracted, fig 5(a). This can be conveniently studied using a Poincare map :

$$\Phi: C \rightarrow C, \quad \Phi(\theta) = \theta' \quad [1.26]$$

which maps a cross-section  $C$  of a flow into itself in the neighborhood of a periodic orbit by following the flow until it intersects the cross section again, fig 5(c). This results in an iteration on the cross section  $C$  in which points are mapped to their positions one cycle later. This is sometimes called a *phase portrait* because the mapping arises from the effect of a phase shift in the oscillation on the closed orbit.

The Poincaré map of a two-dimensional flow on the torus with angular frequencies  $\omega_1$  and  $\omega_2$  results in a rotation of the circular cross section by an angle  $\Omega = \frac{\omega_2}{\omega_1}$ . Adding a small perturbation  $\varepsilon f(\theta_n)$  we get :

$$\theta_{n+1} = \Phi(\theta_n) = \theta_n + \Omega + \varepsilon f(\theta_n) \text{ mod } 1 \quad [1.27]$$

If  $\Omega$  is rational, i.e.  $\Omega = \frac{a}{b}$ , a, b integer, the orbits are periodic and meet themselves again, fig 5(b) after b cycles through C. However if  $\Omega$  is irrational, the orbits pass arbitrarily close but never meet, fig 5(c) and are called *quasi-periodic*. Each orbit is then dense and ergodic on the whole torus.

Further bifurcation to form a third frequency will generally lead to collapse of the corresponding 3-torus to form a strange attractor. Like the intermittency route, this results in chaos after only a finite sequence of bifurcations. It differs from the other two however in the increase in the dimensionality of the attractor with each bifurcation.

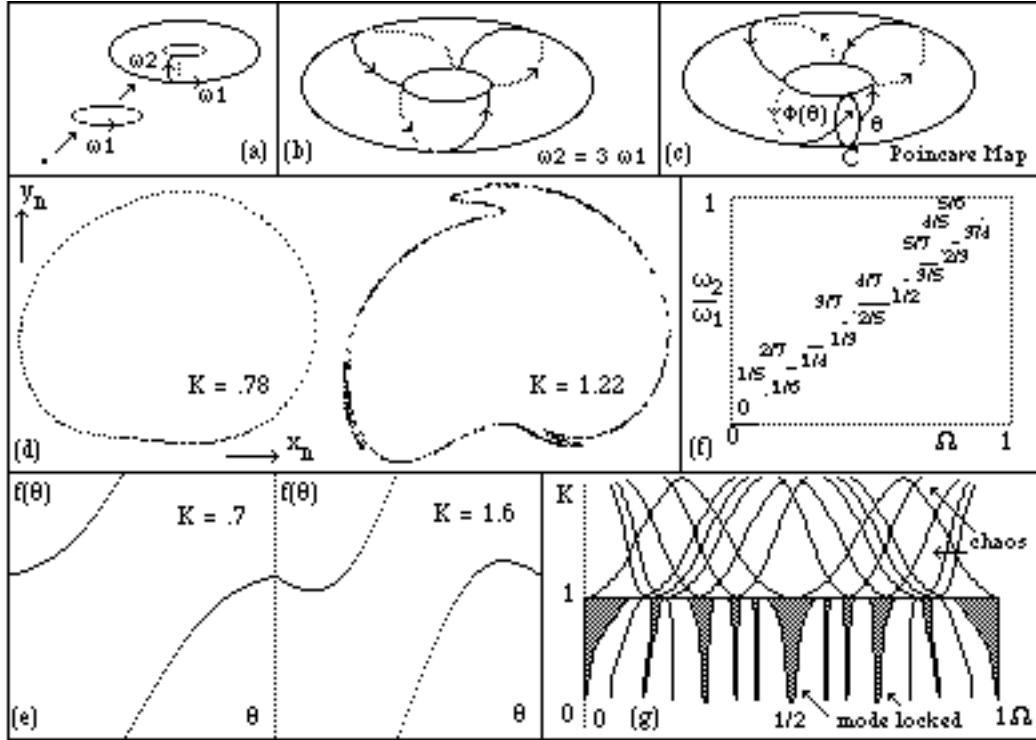


Fig 5 : (a) Repeated Hopf bifurcations result in tori. Creation of two oscillations results in a flow on the 2-torus.  
 (b) Periodic flow on 2-torus results in closed orbits which meet themselves exactly.  
 (c) Poincaré map of a cross section maps each point in a cross section C to the corresponding point one cycle on along the flow. The flow illustrated is irrational and hence has orbits consisting of lines which do not meet themselves, but cover the torus ergodically passing arbitrarily close as time increases.  
 (d) Breakup of the torus under the circle map as K crosses 1.  
 (e)  $f(\theta)$  versus  $\theta$  for the circle map. At  $K = .7$  the function is 1 - 1 and hence invertible, but for  $K = 1.6$  it is not.  
 (f) The devil's staircase of mode-locked states. These order the possible rationals assigning to each the interval of values for which such mode-locking occurs for  $K = 1$ .

At this value the mode-locked states fill the interval, leaving only a Cantor set of irrational flows.

(g)  $K - \Omega$  diagram of the circle map showing mode-locked tongues ( $K < 1$ ) and chaos densely interwoven with periodicity ( $K > 1$ ). The rational mode-locking exist only on the curves for  $K > 1$ .

Study of this breakup can be facilitated by examining the dissipative circle map derived from a periodically excited rotator (Schuster 1986):

$$\theta_{n+1} = \theta_n + \Omega - \frac{K}{2\pi} \sin(2\pi\theta_n) + br_n \text{ mod } 1 \quad [1.28a]$$

$$r_{n+1} = br_n - \frac{K}{2\pi} \sin(2\pi\theta_n) \quad [1.28b]$$

In fig 5(d) is shown the cross section of the torus determined by this map and its breakup as K crosses 1. The variables are  $x_n = (1+4r_n) \cos(2\pi\theta_n)$  &  $y_n = (1+4r_n) \sin(2\pi\theta_n)$ .

This map reduces with  $b \rightarrow 0$  (high dissipation) to:

$$\theta_{n+1} = \theta_n + \Omega - \frac{K}{2\pi} \sin(2\pi\theta_n) \text{ mod } 1 \quad [1.29]$$

This is simply a special case of the circle map of [1.27]. The *sin* term can be replaced by any periodic function which possesses the transition shown in fig 5(e) from a 1-1 function which is invertible, to a non-invertible form.

The development of chaos with increasing K is as follows ( see fig 5(f,g) ) :

(1) **Mode locking** : As K varies from 0 towards 1, a set of intervals of relative frequency  $\Omega$  occur on which the dynamic is mode-locked into rational frequency relationships, called *Arnold tongues*. Between these there is an irrational flow. Both irrational and rational cases have non-zero measure. Universal scaling properties similar to [1.25] occur locally for  $\Omega_n$  values approaching the golden mean and globally for the tongue widths.

(2) **Devil's staircase** : At K = 1 these tongues fill the interval, leaving only a Cantor set of  $\Omega$  values of measure zero and fractal dimension 0.85 with irrational dynamics. These form the Devil's staircase of ordered rational values as shown in (f), in which successive rationals each have an interval over which resonance occurs.

(3) **Chaos & Order** : For K > 1 chaotic and non-chaotic regions are densely interwoven in K- $\Omega$  parameter space. This means that any state neighbors both chaotic and quasi-periodic states. For each rational mode-locked state there are two curves in parameter space which retain the cycle length of the mode-locked case.

(iii) **Conservative Systems and the Mixing Process.** The involvement of chaos in turbulent dissipative systems does not stop conservative systems displaying chaotic dynamics. In particular, in conservative dynamical systems, the lack of attractors leads to structurally unstable configurations in which chaos and quasi-periodic motion can coexist in the same system depending on the initial conditions. In fig 6(a) a single value of the parameter gives both periodic orbits (ellipses) and chaotic orbits (stippled areas).

Conservative systems have similar mode-locking to the dissipative case, except that here the rational frequencies give rise to fractal Cantor-tori and chaos. In fig 6(a) below, is shown the Chirikov map which forms the discrete integral of a conservative rotator periodically kicked by a sinusoidal potential:

$$p_{n+1} = p_n - K \sin(\theta_n), \quad \theta_{n+1} = \theta_n + p_{n+1} \quad [1.30]$$

equivalent to the Poincaré map of a continuous system. Poincare maps of conservative systems generally include homoclinic (self-seeking) or heteroclinic orbits joining unstable saddles at hyperbolic fixed points, as in fig 6(c). Hyperbolic and elliptic fixed points run vertically down 6(a) forming X and O centres respectively. For K < 0.972, the orbits with momenta between p- & p+ remain confined and separate the chaotic stippled regions on either side. For k = 1.13, a different pattern emerges with the chaotic region becoming joined by a fractal boundary. This makes possible a phenomenon called **deterministic diffusion**, in which the momentum can wander in value with time.

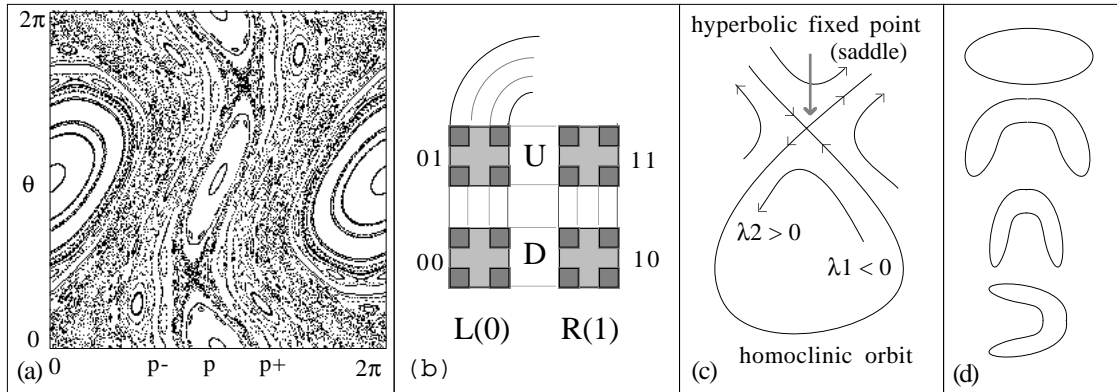


Fig 6 : (a) Chirikov map (K = .9716) displays both chaotic and quasi-periodic orbits at a given energy. Note the elliptic fixed points (surrounded by stable elliptic orbits), hyperbolic fixed points (forming X's down the centre), and chaotic orbits (stippled) all coexistent in a single system. (b) Smale horseshoe map, illustrating the fractal nature of the mixing process. (c) Homoclinic (self-inclined) hyperbolic fixed point, (d) Folding process in the Henon map.

A final important attribute of chaotic systems is the fractal nature of the mixing process. In the two-dimensional illustration of the **Smale horseshoe** (Holmes 1988), fig 6(b), a map is approximately linear in two regions U & D which are mapped firstly by a linear squeezing of the square horizontally and then a linear stretching and folding over, so that U is mapped on to R and D onto L. Hence a portion of L(=0) is mapped over each of L & R, and similarly for R(=1). This results in a fractal Cantor subset which is mapped indefinitely within itself. Because an element of this subset can be associated with every infinite sequence 0101110. . . etc. , the structure must contain periodic orbits of every period, such as for example 001001. . . , non-periodic orbits corresponding to any random sequence, and even a single dense orbit which can be constructed by writing the binary digits in sequence 0.1.10.11.100.101. . . Note also that the Liapunov exponents  $\lambda_1$  contracting, and  $\lambda_2$  stretching guarantees that

$\lambda_1 < 1 < \lambda_2$  causing an unstable saddle. A homoclinic saddle as in (c) is generally associated with a horseshoe, which in turn is an indicator of chaos. The logistic map for  $r > 4$  provides a one-dimensional example of a horseshoe Cantor set, fig 2(d).

The Henon map 
$$x_{n+1} = 2.124 - x_n^2 - 0.3 y_n, y_{n+1} = x_n \quad [1.31]$$

carries out a very similar process to the horseshoe construction. It can be decomposed into an area-preserving bending, followed by lateral contraction and a rotation, as illustrated in fig 6(d).

#### (d) Quasiperiodicity, Stochasticity & Chaos

It is important to be able to distinguish chaotic systems from systems which may have both multiple periodicity and a degree of external noise or stochastic behavior. We have seen that the presence of external noise suppresses the higher-order periodic attractors, thus requiring further tests to eliminate hidden periodicities.

The power spectrum is one measure of the difference between chaos and quasi-periodic motion. The Liapunov exponent can also be used. In a purely stochastic process in which  $x_n$  is subsequently distributed randomly across all possible values of  $x_{n+1}$ , the Liapunov exponent will be  $\infty$ . By contrast, in a quasi-periodic system with many periodic attractors, the Liapunov exponents should all be less than 1. For chaotic systems some of the Liapunov exponents should have positive finite values. These can be calculated indirectly as follows: We firstly use an  $x_{n+1}, x_n$  plot of a time-series to build up a profile of the transfer function  $x_{n+1} = G(x_n)$ . We then use this graph to make an empirical calculation of  $G'(x)$ . Finally we can use [1.7] to get  $\lambda$  (see fig 13(d)). Existence of chaos can also be established by demonstrating a period 3 orbit, fig 13(d) and applying the previously result that period 3 orbits imply chaos. Because the quasiperiodicity route to chaos requires only three interacting frequencies, non-linear systems with multiple frequencies have a high probability of entering a chaotic regime.

The attractor dimension also gives a measure as uncorrelated random variables should have correlation dimension  $\infty$ . In practice however, because the variables are not completely uncorrelated, dimensions under about 7 provide evidence for deterministic chaos as opposed to purely stochastic behavior fig 16(a). Great care has to be taken however to distinguish chaos from quasi-periodic signals with perturbing noise.

*Singular value decomposition* of the matrix of vectors  $\mathbf{x}_n = x_n, \dots, x_{k+n}$  can reveal periodicities or chaos in

seemingly random time series. The matrix  $A_{N \times k} = \begin{bmatrix} x_1 & x_2 & \dots & x_k \\ x_2 & x_3 & \dots & x_{k+1} \\ \dots & \dots & \dots & \dots \\ x_N & x_{N+1} & \dots & x_{N+k} \end{bmatrix}, N \geq k$

can be diagonalized  $W_{k \times N}^T \cdot A_{N \times k} \cdot U_{k \times k} = S_{k \times k}$   $U, W$  orthogonal:  $U \cdot U^T = 1, W^T \cdot W = 1$ , [1.32]

Where the diagonal entries in  $S$  satisfy  $s_1 \geq s_2 \geq \dots \geq s_k \geq 0$  and  $U$  is a rotation in  $k$ -space (Albano et. al. 1986b)

Hence applying this rotation to the vectors  $\mathbf{x}_n$  to get  $\mathbf{x}_n^R$  should not change the correlation dimension.

Since the rotated vectors  $\begin{bmatrix} \mathbf{x}_1^R \\ \dots \\ \mathbf{x}_N^R \end{bmatrix} = A_{N \times k} \cdot U_{k \times k} = W_{N \times k} \cdot S_{k \times k} = \begin{bmatrix} s_1 w_{11} & \dots & s_k w_{1k} \\ \dots & \dots & \dots \\ s_1 w_{N1} & \dots & s_k w_{Nk} \end{bmatrix}$  [1.33]

in the event that the singular values  $s_i$  have an abrupt order of magnitude decrease after  $s_j$  then the rotated vectors can be reduced to their first  $j$  components. This method can sometimes unveil low-dimensional or quasi-periodic dynamics with perturbing noise as opposed to high-dimensional noise, as illustrated in fig 7 in which rotation using singular decomposition reduced the dimension from unsaturated ( $d_2 > 7$ ) to about 2.6 (Albano et. al. 1986b).

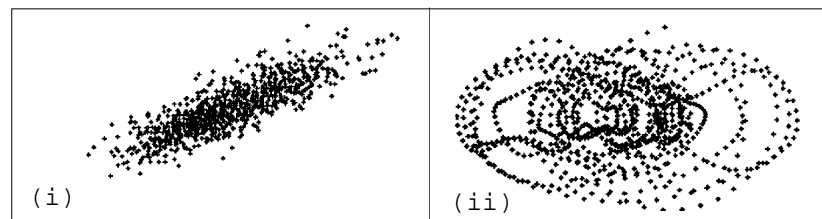


Fig 7: Singular decomposition rotation converts noisy  $x_{n+1} - x_n$  plot (i) into near quasi-periodic  $x_{n+1}^R - x_n^R$  plot (ii).

Singular value decompositions can under suitable conditions be used on their own to estimate dimensions, but several systems such as the logistic and Henon maps do not give easily-separated singular values (Mees et. al. 1987). An alternative strategy to improve time series estimates of correlation dimension is to use singular-value

decomposition to rotate the vectors and choose a cut-off in the singular values at for example  $10^{-4}$  (Albano et. al. 1988) and subsequently vary the window length in the  $\log C(\epsilon) - \log \epsilon$  plot to maximize the slope plateau.

**(e) Chaos at the Quantum Level and Reduction of the Wave Packet.** Quantum systems differ fundamentally from the classical case. While the evolution of the system proceeds according to a deterministic Hamiltonian equation :

$$(\partial^2 / \partial t^2 - \nabla^2 + m^2) \phi = 0, \quad [1.34]$$

creation and destruction of quanta, particularly in the measurement process, result in causality violations in which the probability interpretation

$$P = \phi^* \cdot \phi \quad [1.35]$$

constitutes the limits on our knowledge of the system. This results in a **stochastic-causal** model, in which measurement collapses the wave function from a superposition of possible states into one of these states. While quantum-mechanics predicts each event only as a probability, the universe appears to have a means to resolve each reduction of the wave-packet uniquely, which I will call the *principle of choice*. This is the subject of Schrödinger's famous cat paradox, in which quantum mechanics predicts a cat killed as a result of a quantum fluctuation is both alive and dead with certain probabilities, while we find it is only one : alive, or dead!

Repeated attempts to model a variety of quantum analogues of classical chaotic systems have revealed significant differences which prevent the full display of chaotic dynamics. For example, the quantum kicked rotator, the analogue of the Chirikov map displays two types of solution, one rationally periodic with a parabolic gain in energy, and the other irrational with only non-diffusive almost-periodic motion. Quantum tunneling (Giesel et. al. 1986) and level repulsion (Schuster 1986) both tend to inhibit the chaotic dynamics of such systems .

The case of the Hydrogen atom in a microwave field (Casati et. al. 1986, Pool 1989) gives the closest approximation to chaos, including quantum diffusion. However numerical simulation of the quantum system remains entirely time-reversible and will regain the initial conditions, for example by phase reversal of the Fourier expansion, unlike the non-reversibility of the classical solution. Laser stimulation of molecules such as acetylene (Pique et. al. 1987) also displays borderline chaos in the fine spectra, supporting the notion that more complex molecules may display quantum chaotic phenomena under stimulation.

However it is the stochastic wave-reduction aspect of quantum mechanics which appears to underpin the uncertainty found in classical chaos. The statistical mechanics of molecular systems ultimately derives its randomness from

Heisenberg uncertainty 
$$\Delta E \cdot \Delta t \sim \frac{\hbar}{2\pi}, \quad \Delta p_x \cdot \Delta x \sim \frac{\hbar}{2\pi} \quad [1.36]$$

in the form of wave-packet reduction. The position of a molecule is thus uncertain as a result of the spreading of its wave function. This uncertainty is unstably reflected in subsequent kinetic encounters causing  $\epsilon$ -small perturbations of a classically chaotic system. One of the important roles of classical chaos may thus be the amplification of quantum uncertainty into macroscopic indeterminacy. Ultimately sensitive-dependence in classical systems will result in **quantum inflation**, the amplification of quantum fluctuation into global perturbations of the dynamic.

## 2 : The Modelling of Neural Systems

### (a) Computational Processes and Causal Closure

Generally, a computational process is designed to be determined by the input conditions and the algorithms within the program so as to arrive at a logically precise outcome. A computer program which fails to conform to such criteria may crash, or give unreliable results. The inclusion of random variation within such a system is normally associated with noise or component failure and is avoided.

These criteria are softened in certain artificial intelligence approaches in which a computational system is required to handle input from an open system, where the external conditions being responded to may not yield to a single deterministic algorithmic strategy. A heuristic approach is then followed in which differing strategies are adopted with differing probabilities which may be a function of previous successes.

A second limitation on deterministic algorithmic processes is caused by problems which are *intrinsically difficult*, because deterministic processes require exponentiating computation times as the number  $n$  of cases increases. An example is the travelling salesman problem, which involves finding the minimum cyclic path joining  $n$  points, fig 9. A simple estimate of the number of cases involved is  $n!/2n$  since the  $n!$  cases are divided by  $n$  equivalent starting points and two directions of travel. This involves 12 possibilities for 5 points, 181,400 for 10 points, and  $3.09 \times 10^{23}$  for 25 points, taking  $10^9$  years at a million cases a second. Problems that scale like  $n^k$  as the number  $n$  increases are *tractable*, while ones scaling like  $e^n$  are intrinsically difficult (Cowan et. al. 1988, Bern et. al. 1989).

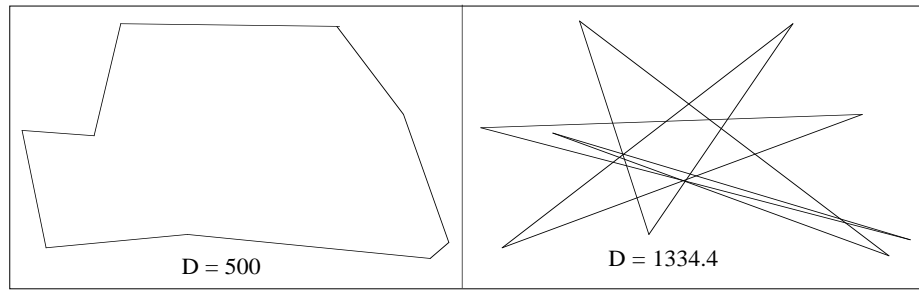


Fig 8 : Travelling salesman problem for 9 vertices. Maximal and minimal paths.

A final limit on computability exists in the consequences of Gödel's theorem determining that some logical propositions may be *formally undecidable* from within the axioms of the system in which they are constructed. A *Turing machine* is a formal computer with potentially infinite memory operating on binary data. Turing has proved that it is formally undecidable whether a Turing machine will in fact complete a calculation determined by a given input code. This raises serious questions as to the logical completeness of computability in general. Roger Penrose has pointed out that the entire program of strong artificial intelligence in which conceptual models of the brain are based on formal computing models and axioms may thus be doomed to failure (Penrose 1989, Searle 1987, 1990, Churchland & Churchland 1990).

Spin glasses (Cowan 1988, Stein 1989) are materials with chaotically oriented atomic spins which can reach neither a ferromagnetic equilibrium (spins aligned) nor a paramagnetic one (spins cancelling in pairs), because of long-range spin interactions between magnetic trace atoms (Fe) and the conduction electrons of the host material (Cu). Because these effects reverse repeatedly with distance, no simple state fully resolves the dynamics, and spin glasses thus adopt a large variety of disordered states. Modelling the transition to a spin glass has close parallels in neural nets, particularly the Hopfield nets consisting of symmetrically unstable circuits. Optimization of a task is then modelled in terms of constrained minimization of a potential function. However the problem of determining the global minimum among all the local minima in a system with a large number of degrees of freedom is intrinsically difficult. Spin glasses are also chaotic and display sensitive dependence (Bray & Moore 1987). Similar dynamics occurs in simulations continuous fields of neurons (Cowan & Sharp 1988).

*Annealing* is a thermodynamic simulation of a spin glass in which the *temperature* of random fluctuations is slowly lowered, allowing individual dynamic trajectories to have a good probability of finding quasi-optimal states. Suppose we start out at an arbitrary initial state of a system and follow the topography into the nearest valley, reaching a local minimum. If a random fluctuation now provides sufficient energy to carry the state past an adjacent saddle, the trajectory can explore further potential minima. Modelling such processes requires the inclusion of a controlled level of randomness in local dynamical states, something which in classical computing would be regarded as a leaky, entropic process. The open environment is notorious as a source of such intrinsically difficult problems, which may have encouraged the use of chaotic systems in the evolutionary development of the vertebrate brain.

One of the most important aspects of the design of flexible algorithmic process is a modular architecture in which new routines can be added to the existing repertoire in the event that existing strategies cannot provide an effective solution, even if this is at the level of a primitive. Such a system must have the capacity to generate variation at any level of processing.

A classical deterministic system following the principles of the Laplacian universe can be described by specifying its equations of evolution and the initial conditions. Often the equations of evolution take the form of differential equations. The classical Hamiltonian and Lagrangian dynamical equations, for example, are both expressed as differential equations defining generalized coordinates as a function of increasing time, where  $\mathcal{L} = T - V$  and similarly  $\mathcal{H} = T + V$ , giving the total (T kinetic & V potential) energy :

$$\frac{d}{dt} \left( \frac{\partial \mathcal{L}}{\partial \dot{q}_i} \right) - \frac{\partial \mathcal{L}}{\partial q_i} = 0 \quad i = 1, \dots, N \quad [2.1]$$

$$\mathcal{H} = \sum_i p_i \dot{q}_i - \mathcal{L} \quad \frac{\partial \mathcal{H}}{\partial p_i} = \dot{q}_i \quad \frac{\partial \mathcal{H}}{\partial q_i} = -\dot{p}_i \quad [2.2]$$

We will call such a system **causally closed** because it obeys strict causality in time, and is completely specified by its initial or other boundary conditions. By contrast, a system which is not closed may display non-deterministic behavior, resulting from information which enters the system during its time evolution. We will call such a system **causally open**. A partially random process, such as a Markov process is causally open. At a deeper level, the **stochastic-causal** processes of quantum mechanics are also causally open because Heisenberg uncertainty [1.36] prevents a complete causal description of quantum dynamics. The probability interpretation of the wave function



and a suitably wired net will move exponentially towards a solution close to the minimum distance connecting them. Although the total number of such quasi-optimal local minima is restricted by spin glass theory to approximately the number of cells, the system runs into the classical problem of multiplying local minima as the number of cases grows large. The solution also results from a careful choice of synaptic weightings to define the problem as a minimization rather than a learning process.

To avoid having to test all the configurations of the state space, a strategy like annealing in spin glasses can be used. A trajectory from a given initial state is followed to a local minimum. The state of a given unit is then randomly reversed and the new state is retained if it is optimal over the unreversed configuration. Such a net is then termed a *Boltzman machine*. Multi-layered perceptron and Hopfield nets can be trained to perform several sensory pattern-recognition tasks such as character recognition.

More efficient adaptation and a solution to the XOR problem arises from *back-propagation* as illustrated in fig 9(c). The neurons are amplifiers with a linear gain  $G$ , and modification occurs in 2 stages elaborating the adaline rules :

$$\begin{aligned} \text{(i)} \quad \Delta w_{jk} &= h_j \varepsilon_k(s) G(m_k) \\ \text{(ii)} \quad \Delta W_{ij} &= s_i G(h_j) \sum_k w_{jk} \varepsilon_k(s) G(m_k) \end{aligned} \quad [2.6]$$

Chaos does not exist in these dynamical models because of the symmetry in synaptic weightings, which ensures the models are designed to stably seek local minima, however the systems are dynamically capable of chaos if symmetry is removed. It should be noted that chaotic pacemaker and silent cells of the PLMI type can be used to model periodic neural nets, making it possible for chaotic neurons to give rise to periodic circuits (Labos 1986).

**(c) The Adaptive Resonance Architecture.** One of the most interesting neural net models is the ART or *adaptive resonance theory* model of Grossberg (1983,1987,1988). The system consists of a set of two coupled neural nets, which are capable of developing self-directed pattern recognition without the problems of entrapment in local minima, memory saturation, requirements for external guidance and resetting of other nets. The general configuration of the ART system is shown in fig 10(b). This consists of two fields of formal neurons. The field  $F_1$  receives the input pattern of 0's and 1's, which is passed via synaptic connections to the upper field  $F_2$ .  $F_2$  has mutual (dipole) lateral inhibition, fig 10(a), which causes contrast enhancement and in the ideal case determines a winner-take-all strategy in which only the maximally-excited node is activated. Such activation will then result in the top-down synapses back to  $F_1$  activating the learned pattern represented by this node.

Gain controls enable the lower field to respond to the full bottom-up input pattern if  $F_2$  is inactive, but only to the intersection of the bottom-up and top-down features if  $F_2$  is activated, permitting both generalization of a set of features and mismatch masking. The two thus form an **attentional subsystem** which through such masking can detect match or mismatch between the input and top-down model. In the event of match, the intersected model is reinforced, but in the event of mismatch, a second feedback system, the **orienting subsystem** takes over and resets the given node in  $F_2$  so that it is below the other thresholds. In this manner the system beginning with the input, will sequentially seek a node which either represents the input within tolerance, or is free to be used as a template for the pattern presented. Only then does pattern discrimination learning take place. Other refined modulation varies the synaptic adjustments inversely with pattern complexity so that complex patterns with only minor (random) variation are clumped while simple patterns with significant variation are discriminated.

The system also captures characteristics of short-term (STM) and long-term memory (LTM). The short-term memory resides in the dynamic activity of the each layer. Long-term memory results from changes in the synapses once a stable representation of the input has been formed. A more advanced version, the ART2 (Carpenter & Grossberg 1988) has three  $F_1$  fields to hold input and masked patterns separately and is capable of pattern discrimination learning of continuous analog inputs once they are converted into digital form.

The strengths of the model are that it has been developed by a mutual investigation of biological feature detection systems and theory of parallel distributed networks, and thus forms a relatively good model of biological systems, that it is capable of self-organization and is less subject to the difficulties associated with constrained optimization. The model has been used to successfully predict a variety of aspects of central nervous behavior from word-length effects in word recognition to a hippocampal generator for the P300 event-related potential, consistent with a role of the hippocampus in cortical memory formation. One weakness is that the system depends on *digital* processing of features which are *pre-defined*. Although the visual system has prominent detector types, the same generalizations have not been made so clearly for example in olfaction. Moreover there is some evidence that the structure of visual processing is at least partially dependent on the dynamics of input (Kalil 1989).

The versions of ART form one of the best model systems yet devised of active pattern recognition, which has, at least in germinal form many of the observed functional aspects of biological nervous function. It is thus a valid foil with which to compare chaotic models. Although the model is digital and is thus not formally capable of chaotic dynamics, its functional characteristics could lead to chaotic dynamics in continuous versions. In particular, the

dipole mutual inhibition and selection of optimal nodes should lead to structurally unstable dynamics. The intervening phases of sequential search with orienting reset and stable attentional learning should result in dynamics with sensitive dependence typified by the loss of phase coherence during unfamiliar stimuli followed by coherence once familiarization has occurred as discussed later. Thus although the ART model is in a sense a competitor to chaotic models such as those of Freeman, to be discussed later, the two may in actuality be complementary perspectives on a common biological mechanism, both of which are simplifications of real systems.

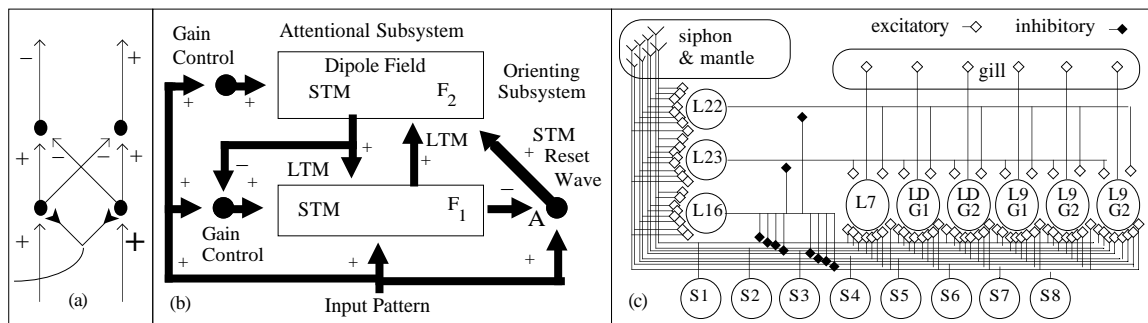


Fig 10 (a) A Gated Dipole involves mutual inhibition between two competing excitatory pathways.

Such an arrangement is characteristic of contrast-enhancement and can lead to dynamical instability.

(b) The Adaptive Resonance Network involves two layered nets each with gain controls forming an attentional subsystem. Repeated search and mismatch detection governed by a second, orienting subsystem enables self-organized pattern recognition learning. The system also has short term (dynamic) and long term (synaptic) memory.

(c) Siphon - Gill connections in *Aplysia* showing excitatory and inhibitory interneurons.

**(d) Comparison with Biological Nerve Nets.** Systems of biological neurons both in simpler animals such as the sea snail *Aplysia*, and in models of higher nervous systems such as Marr's model of the cerebellum fig 13(b) display a similar architecture to such formal nets in important ways. The architecture of biological neural systems comprises a layered parallel circuitry in which only a small number of synapses occurs between input & output. The parallel architecture is modulated by several interneuron cell types, each having distinct neurotransmitters, resulting in excitatory and particularly inhibitory feedback, and threshold modulation. In Marr's model of the cerebellum fig 13(b) (Marr 1969, Cowan 1988) several inhibitory interneurons such as basket and stellate cells act to modulate the connection between the incoming mossy fibres and Purkinje cell output via excitatory synapses between the granule and Purkinje cells, which are thus entrained by climbing fibre input. The Golgi cells then modulate the level of activity of the granule cells to prevent overload and the other interneurons modulate the Purkinje cells to ensure recall of stored data rather than random excitations. The entrainment is believed to *weaken* the synapses which are entrained, so as to remove Purkinje inhibition from the cerebellar nucleus. The model has not been definitively tested for validity. It does not include the active masking and feedback of the ART configuration, and considers only long-term changes rather than dynamical features. Nevertheless the architecture of such inhibitory interneurons is capable of generating structural instability through modulation of transverse inhibitory connections.

Modular feature detection units such as the line-orientation, and ocular-dominance columns in the visual cortex (Hubel & Wiesel 1979) appear to have a similar, although more elaborate structure resulting from the 5 - 6 layers of the 20 or so neuron types in each unit. The form of the chaotic model of Freeman fig 16(b) hypothesizes a series of such parallel units linking the olfactory bulb (OB), pyriform cortex (PC) and entorhinal cortex (EC). Each of these units has a parallel architecture with a combination of positive and negative feedback leading to dynamical behavior similar to the experimental EEG fig 16(d).

In the abdominal ganglion of the *Aplysia* (Kandel 1979) in which each neuron has a distinct genetically programmed function, a strongly parallel architecture connects sensory input in the siphon to motor action in the gill with a set of three interneurons, two excitatory and one inhibitory, fig 10(c). Notably in *Aplysia* identifiable master cells such as the cardiac regulator have intermittent firing patterns consistent with sensitive dependence and chaos rather than the regular beating or bursting patterns characteristic of lower level neurons. Facilitation is also mediated by synapto-synaptic junctions as in fig 13(a).

Chaos may be characteristic of periodic feedback loops which require in addition sensitive plasticity to external modulations. Chaotic feedback loops may thus be a very general phenomenon common for example to the cortico-thalamic links in the alpha rhythm, the limbic system and the orienting reaction, as well as pattern recognition in sense perception. The combination of such feedback with the mutual (dipole) inhibition characteristic of contrast enhancement leads to structural instability. Mutual global-local coupling between the dynamics of neurosystems and that of single neurons is notable in its potentiality to couple cellular and neurosystems instabilities (Alkon 1989).

### 3 : The Diversity of Non-linear Characteristics of the Neuron and Synapse

**(a) The Neuron** The functional response of a neuron is generally compared to a linear integrator in which the firing rate is proportional to the sum of the synaptic inputs. The purpose of this section is to illustrate how far the neuron diverges in actuality from this simple linear model, by investigating the varieties of non-linear behavior in

the neuron and synapse.

The integrative character of the neuron naturally leads to models in which *transforms* represent the integrative function. Suppose successive layers  $n$  and  $n+1$  in a net, have a fixed serial excitation, and lateral inhibition which is normally distributed according to the function  $e^{-kx^2}$ . We can then define the following integral transform :

$$f_{n+1}(x) = f_n(x) + \int_{-\infty}^{\infty} e^{-k(x-\chi)^2} \{f_n(x) - f_n(\chi)\} d\chi \quad [3.1]$$

as a model in which the first term is excitation and the integral is a type of convolution between the normal distribution and changing levels of excitation. Numerical computation of the effect of this transform on the Heaviside step function, demonstrates contrast enhancement as a result of continuous lateral inhibition. A somewhat different convolving function is needed to provide easy inversion as in the Fourier transform :

$$F(\omega) = \int_{-\infty}^{\infty} f(t) e^{-i\omega t} dt \quad \text{and its inverse} \quad f(t) = \frac{1}{2\pi} \int_{-\infty}^{\infty} F(\omega) e^{i\omega t} d\omega \quad [3.2]$$

to model memory recall. Modification of the exponential term, through graded excitatory and inhibitory synapses, for example into an inverse Fourier transform of a step function (Crick et. al. 1988) could generate such a model. The LTM synapses of the ART configuration similarly have characteristics of mutually-inverting transforms.

Both the dynamics of excitatory and inhibitory synapses and the specific details of the transmission response display clear-cut non-linear behavior. To quote Jack, Noble & Tsien (1978) "the range of potentials over which the membrane may be assumed to be linear is very restricted". The non-linear nature of some cellular components such as the synapse are less well explored . . . "Only moderate progress has been made so far in developing mathematical techniques which might suggest ways of making an experimental determination of the electrical geometry of a particular nerve cell . . . One reason is that the the nerve cell only easily allows recording (or intracellular current passage) from one site - the cell body".

Prominent non-linearities that are well-known in the neuron are the exponentially-derived sigmoidal excitation curve [2.5], and the limit cycle resulting from the  $\text{Na}^+$  and  $\text{K}^+$  current responses to potential that is responsible for the generation of the action potential oscillation, fig 11(aii). The net current is notable in having an S-shaped curve with three zeros. The Hodgkin-Huxley equation [4.8] is specifically non-linear, as it includes power terms  $m^3h$  and  $n^4$ . This is extended in the Chay-Rinzel equation [4.9] to a fully chaotic equation. The response of touch receptors, fig 11(c), (Eccles 1966) illustrates the non-linear nature of excitation with membrane distortion.

Sigmoidal excitation combined with the action limit cycle results in instability, in which slight transitions from below to above threshold result in qualitative transformation from the non-firing state to the state in which at least one action potential will be emitted, fig 11(aii). Beyond the threshold, the rate response is approximately linear with input depolarizing current, fig 11(ai). Similar approximate linearity occurs over a restricted range in conversion of an action potential into a graded potential (Freeman 1983). However non-linearities enter in a variety of ways which cause both the broad periodicities of EEG rhythms and the intermittent chaos of single neurons.

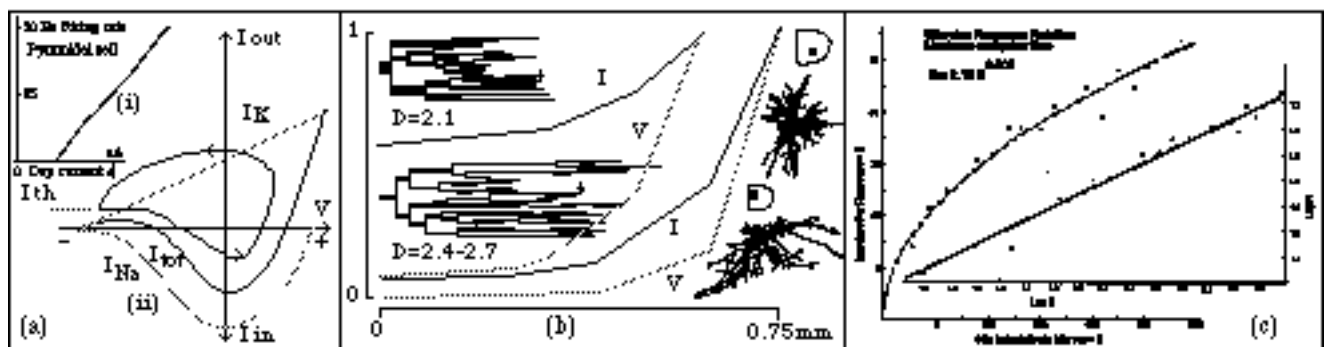


Fig 11 : (ai) Piecewise-linear response of a Pyramidal cell to depolarizing current.

(aii) S-curve of current flow with voltage results from the sum of  $\text{Na}^+$  and  $\text{K}^+$  currents.

The resulting action limit cycle has an abrupt threshold  $I_{th}$  at which the cycle triggers.

(b) Fractal structures of superior colliculus dendrites & the exponential decline of  $I$  &  $V$  with distance.

Note the improved current characteristics of the tree with a lower fractal dimension.

(c) Non-linear (approximately inverse quadratic) response of touch receptors, indicating a general non-linear response to membrane deformations.

The dendritic tree is an obvious example of a fractal structure in neurobiology (Schierwagen 1986). The growth

pattern of dendritic trees has been successfully described by a diffusion-limited aggregation model (Sander 1987), common to several fractal deposition processes. Differing fractal dimensions ranging from 2.1 through to 2.7 result from the diverse anatomies of different cell types. A lower dimension results in fatter dendrites and a higher current transfer, fig 11(b). The continuous dendrite voltage declines exponentially with distance, and the current shows a related fall-off. The combination of excitatory and inhibitory influences is thus spatially dependent, with some synapses occupying strategic positions at the base of particular dendrites. Dendritic and synaptic growth and atrophy with learning cause long-term dynamic change. In the 'twitching spines' concept (Crick 1982), changes in the spines may occur over milliseconds.

The structure of a pyramidal cell neuron is illustrated in fig 12(a) (Eccles 1966). The total number of excitatory and inhibitory synapses ranges up to 200,000 and covers a variety of regions and structures. Although the neuron clearly has the characteristics of integrating the positive and negative influences of hyperpolarizing (inhibitory) and depolarizing (excitatory) synapses, this function is complicated by the variety of physical types of synaptic structures in a complex neuron, the variety of synaptic contacts made by a single cell with several other cell types, and the varying positions of key synapses with respect to specific dendritic branches and the time-dependent changes accompanying facilitation and learning. Dendo-dendritic connections and synaptic microcircuits make it possible that the neuron is essentially a super-unit carrying out multiple processing tasks, each with non-linear potentialities.

A second striking aspect of the neuron is that the membrane is a two-dimensional electronic surface capable of different connectivity properties from one-dimensional systems. Although the neuron is conceived of as an integrative processing unit, both the synaptic junction and the cell body form independent functional sub-units. The cell body both selectively integrates and also often bifurcates the input between active and passive states through oscillatory instabilities at threshold. Growth of new synaptic spines and rearrangements of specific dendritic trees has been associated with learning and in particular, PKC-mediated memory formation (Alkon 1989, Mishkin & Appenzeller 1988). This may occur in local synaptic microcircuits through the cell body making a sub-activation response to a local associative synapse pair as illustrated in fig 12(b) (Alkon 1989).

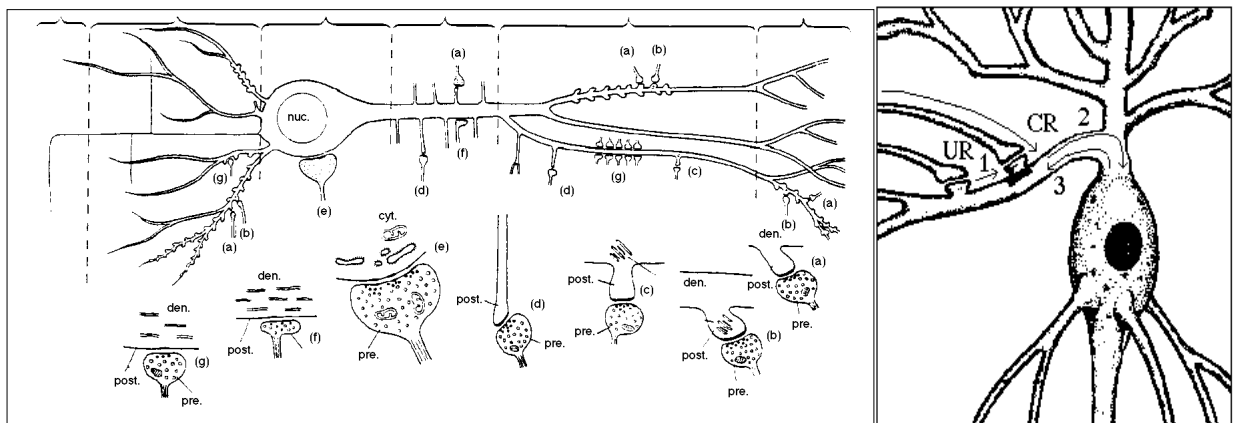


Fig 12 (a) Structure of a pyramidal cell (Eccles 1966) showing the diversity of synaptic types on a single neuron.  
(b) Local fixation of a conditioned response (Alkon 1989) involving dendritic microcircuitry.

The neuron is an amoeboid cell capable of exploratory changes in its dendritic and synaptic linkages which go beyond simple additivity. In at least some species growth of new neurons takes place (Nottebohm 1989). The dynamics of the neuron is complemented by cells such as the oligodendrocytes, which myelinate the axons and the astrocytes which surround neurons in the brain & blood-brain barrier, buffer external  $K^+$  concentration, service synaptic molecules, and may have a role in long-term potential changes (Kimmelberg & Norenberg 1989).

Non-linear aspects of neuronal conduction are essential in the following:

- (1) Discrete decision-making events. Passage past threshold signals "an event" in digital form, causing the unstable bifurcation of continuously varying input into *active* and *passive* states.
- (2) The stability-breaking of mutual (dipole) inhibition in layered nets.
- (3) The development of complex time-dependent dynamics as a consequence of non-linear feedback interactions, for example in loop circuits displaying sensitivity to external input through chaotic excitability.

### (b) The Synapse

Neurons use at least two means to communicate and transfer electrical states from one cell to another. In the electroelectric junction membrane potential is transferred directly, whereas in the electrochemical junction a transduction takes place, involving initial release of neurotransmitting chemicals from the presynaptic membrane, binding of neurotransmitters to receptor sites on the post-synaptic membrane, and subsequent hyper- or de-polarization of the post synaptic membrane. This occurs either by direct effects of the binding protein as an ion channel, or indirectly through the action of second signalling molecules within the cell such as cyclic AMP, which activate a protein

kinase which blocks  $K^+$  flow, thus prolonging depolarization and hence increasing  $Ca^{++}$  inflow (Rasmussen 1989).

Synaptic transduction involves several steps with regulatory feedback. The neurotransmitter is generally stored in membranous capsules called synaptic vesicles similar to those produced by the Golgi apparatus. Depolarization of the synaptic membrane involves both  $Na^+$  and  $Ca^{++}$  channels. The calcium ions promote the binding of the synaptic vesicles to specific receptors on the inside of the pre-synaptic membrane and consequent release of the neurotransmitter into the synaptic cleft. Here the neurotransmitter may bind to an receptor site in the postsynaptic membrane, or to presynaptic receptors which provide feedback control, or be assimilated by enzymes such as monoamine oxidase, which remove surplus neurotransmitters after stimulation, fig 13(a).

As an example, the acetyl-choline receptor at the neuromuscular junction requires two acetyl-choline molecules to activate it (Stevens 1979, Darnell et. al. 1986). A single synaptic vesicle with 10,000 acetyl-choline molecules will activate about 2000 sodium channels, taking about 100 microseconds to traverse the synaptic cleft. Binding of the transmitter lowers the energetic stability of the non-conducting channel resulting in a conformational shift to the open state. After a random interval this will switch to an inactive resting state and finally back to the active resting state when the membrane potential has risen. Such channels may stay open for anything from one millisecond to several hundred depending on the specific type of synapse. About 20,000 ions can traverse an ion channel during the time it is open. Only about 1 in  $10^3$  ions is required to traverse the membrane to shift the potential through the action range. A single synaptic vesicle at the neuro-muscular junction reduces the post-synaptic potential by about 1 mV. Although this is too small to reach threshold, it shows on a recording as a quantized potential spike. By contrast, it has been postulated that some central nervous synapses may function at levels where the order of only one vesicle released will communicate an active state across the synapse, eliciting *quantal* information transfer.

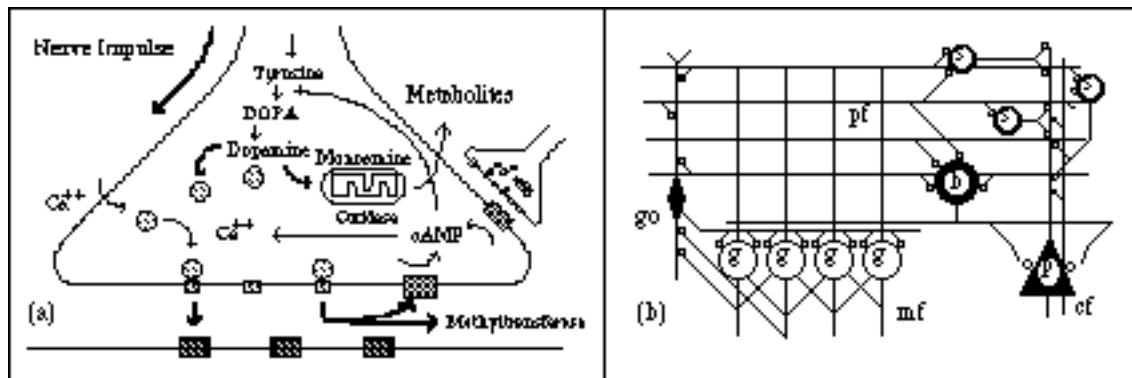


Fig 13 : (a) Neurotransmitter pathways & the synpto-synaptic junction illustrate multiple feedback links and bilinear responses. (b) Marr's model of the cerebellum, showing inhibitory interneuron connection and threshold tuning. [g-granule, go-Golgi, s-stellate, b-basket, p-Purkinje, mf-mossy fibre, pf-parallel fibre, cf-climbing fibre].

In the standard model, neurotransmitter release is quantized through exocytosis of synaptic vesicles. However some neurotransmitters such as acetyl-choline (Cooper et. al. 1982) may also be released without exclusive use of vesicles. The principal action of neurotransmitters is facilitated by binding to receptor sites, which even for a single neurotransmitter such as acetyl-choline may bind to both excitatory (e.g. nicotinic) and inhibitory (e.g. muscarinic) receptors. However the common involvement of choline in both phospholipids and neurotransmitters, combined with the common structures of serotonin & the catecholamines, both of which are derived from aromatic amino acids by specific amine and OH substitutions, suggests that these primitive molecules may have been selected through intrinsic chemical interactions with the non-polar and ionic components of the primitive lipid membrane. The selectivity for amine derivatives may be based, for example, on interactions with primitive ion channels, in which the amine moiety serves to stabilize flow of positive ions (King 1990, Mueller & Rudin 1968).

Equations such as

$$e^{\left(\frac{-\Delta G}{2.303 RT}\right)} = \frac{[P_1][P_2]}{[R_1][R_2]^2} \quad [3.3]$$

display first-order kinetics if a single copy of a given reactant such as  $R_1$  enters the kinetic interaction, as opposed to the two copies of  $R_2$ . However key steps in conversion of excitation, such as neurotransmitter binding to ion channels, require *two* molecules of neurotransmitter per channel and hence behave quadratically like  $R_2$ .

The complexity of synaptic kinetics including presynaptic receptors, lytic enzymes, synpto-synaptic and dendro-dendritic junctions, and microcircuits provide further sources of non-linearity. In fig 13(a) is shown a synpto-synaptic junction in which a neurotransmitter such as serotonin facilitates the sensitivity of an underlying synaptic junction by binding to cyclic AMP producing sites on the main synapse. This subsequently increases the  $Ca^{++}$  concentration and makes the second synapse more sensitive, through making the vesicles more accessible to the surface receptors that promote their emptying into the synaptic cleft. Such synpto-synaptic junctions result in

*bilinear* response characteristics over time intervals, because the post-synaptic potential is a product of pre-synaptic and synaptic inputs

$$V_{\text{out}} \sim k V_{\text{pre}} \cdot V_{\text{in}} \quad [3.4]$$

Such triple junctions may be important in the production of learned responses. Simple nervous systems, such as those in the sea snail *Aplysia* (Kandell 1979), have synapto-synaptic junctions which appear to function in facilitation in learning through this multiplicative effect. Note that the Lorentz system fig 1(a) is purely bilinear.

#### (4) Evidence for Chaos and Fractal Dynamics in Excitable Cells.\

(a) **Membrane electrodynamics** : The Hodgkin-Huxley model of (1952) of the action potential is the foundation of modelling of the dynamical response of excitable cells, and as such has led to the development of the Chay-Rinzel model of the chaotic neuron. To derive the model, we assume that the ionic current for each principal ion  $i = K, Na$  is :

$$I_i = g_i(n_i)(V - V_i) \quad [4.1]$$

where  $g_i$  is a function depending on the proportion  $n_i$  of ions inside the membrane,  $V$  is the displacement from resting potential and  $V_i$  is the standard potential of the ion  $i$ . Generally, the rate of change of  $n_i$  is given by

$$\frac{dn_i}{dt} = \alpha(n_i) [1 - n_i] - \beta(n_i) n_i \quad [4.2]^*$$

where  $\alpha(n_i)$  and  $\beta(n_i)$  are the rate constants for the inward and outward movements of ions for a given  $n_i$  with the proportion outside being  $1 - n_i$ . Since at equilibrium for any given voltage, we have

$$\frac{dn_i}{dt} = 0 \quad \text{we can define steady state } \hat{n}_i = \frac{\alpha(n_i)}{\alpha(n_i) + \beta(n_i)} = \alpha(n_i) \tau(n_i), \quad \text{where } \tau(n_i) = \frac{1}{\alpha(n_i) + \beta(n_i)} \quad [4.3]$$

Let  $\hat{n}_{i0}$  &  $\hat{n}_{i\infty}$  be the equilibrium states before and after clamping with a voltage  $V$ , then

$$n = \hat{n}_{i\infty} - (\hat{n}_{i0} - \hat{n}_{i\infty}) e^{-t/\tau(n_i)} \quad [4.4]$$

The inverse relations to [4.3]

$$\alpha(n_i) = \hat{n}_{i\infty} / \tau(n_i), \quad \beta(n_i) = (1 - \hat{n}_{i\infty}) / \tau(n_i) \quad [4.5]$$

can then be used to calculate  $\alpha$  &  $\beta$  experimentally as a function of voltage, returning, for example, in the case of K

$$\alpha(n_K) = \frac{0.01(V + 10)}{e^{(V/10-1)} - 1}, \quad \beta(n_K) = 0.125 e^{(V/80)} \quad [4.6]^*$$

If a given ion is transported through binding to the channel in  $k$ -tuples, the ionic conductances will obey the power law

$$g_i(n_i) = \bar{g}_i n_i^k \quad \text{for some power } k \text{ of } n_i. \quad [4.7]$$

This can then be put together into a total (capacitative plus ionic) current equation ( $h = Na$  inhibitor,  $L = leakage$ ).

$$I = C_M \frac{dV}{dt} + \bar{g}_K n^4 (V - V_K) + \bar{g}_{Na} m^3 h (V - V_{Na}) + \bar{g}_L (V - V_L) \quad [4.8]^*$$

The asterisked equations [4.2], [4.6] & [4.8] in combination then form the Hodgkin-Huxley system.

It is well known that a variety of excitable cells including in particular the  $\beta$ -cells of the pancreatic islets display action potentials which are capable of both chaotic bursting and a variety of periodic modes of activity. This is caused by the action of glucose lowering intra-cellular  $Ca^{++}$  and appears to involve four components,  $Ca^{++}$  and  $V$  activated  $K^+$  channels, a  $V$  activated  $Ca^{++}$  channel and effects of glucose on  $Ca^{++}$  via ATP. Chay & Rinzel (1985) successfully adapted the Hodgkin-Huxley system by replacing the  $Na$  term with an identical  $Ca$  term and including

the  $Ca$  activated  $K$  channel in :

$$g_K = \bar{g}_K n^4 + \bar{g}_{KCa} \frac{y}{1+y}, \quad y = \frac{Ca_i}{K_{diss}} \quad [4.9]$$

and an extra term

$$\frac{dCa_i}{dt} = \frac{dCa_i}{dCa_T} \left( \frac{3I_{Ca}}{rF} - k_{Ca} Ca_i \right) \quad [4.10]$$

representing the removal of internal  $Ca$  by pumping and its inflow via the  $Ca$  channel.

The dynamical behavior of the model compares closely with the actual activity of such cells and includes in particular a series of regimes as the rate constant for removal of calcium  $k_{Ca}$  is varied upward, including periodic & then chaotic bursts, followed by chaotic & then periodic beating. The periodic beating arises through the period doubling route as in fig 14(f). Since  $Ca^{++}$  is also central in synaptic exchange, such dynamics may generalize to neuronal networks. Similar experimental results occur in neurons. Sinusoidal stimulation of the internodal cells of *Nitella* result in the formation of period 3 bursting and hence chaos (Hayashi et. al. 1982), fig 14(a), and deterministic chaos has also been defined in the activity of single neurons. Enzyme systems such as the glycolytic pathway have likewise displayed chaotic and period 3 dynamics, both in experimental models and in yeast cells under sinusoidal glucose concentrations (Markus et. al. 1985).

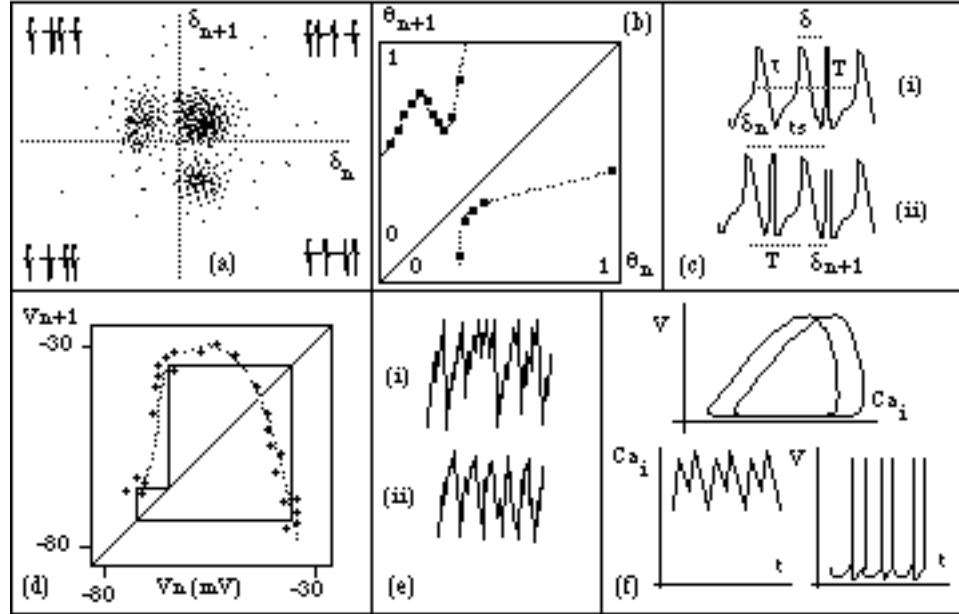


Fig 14 : (a) Clumping in successive periods in ECG is indicative of chaos rather than noise, (Babloyantz 1989). The figure plots successive delays, demonstrating a non-random spread.  
 (b) The form of  $g(\theta)$  in chicken heart cells, from a  $\theta_n - \theta_{n+1}$  plot. This closely approximates the form of the circle map function fig 5(e) justifying the use of the circle map in the model.  
 (c) Periods in chicken heart aggregates used to develop the model in detail.  
 (d) Period 3 attractor in *Nitella*, & interpolation of the transfer function by taking repeated iterates and plotting  $V_{n+1}$  against  $V_n$  to form the analogue of the figures in fig 4(b) for this map.  
 (e) Forms of chaotic waveforms in the Chay-Rinzel model (bursting) & in *Nitella*.  
 (f) period doubling in Chay-Rinzel model (beating) shown by plots of  $V$ ,  $Ca_i$  and  $t$  together.

The circle map is useful in the modelling of chicken heart cell aggregates, which are stimulated by a periodic pulse (Schuster 1986), figs 14(b), 5(d). Like the dynamics of the cortical EEG, the phase shift of the stimulus is the determining parameter in the dynamics. If the natural period is  $\tau$ , the stimulated period is  $T$  and  $\delta$  is the stimulus delay, we find that the function :

$$T/\tau = g(\theta) = g(\delta/\tau) \quad [4.11]$$

has form equivalent to the circle map, and by examining a single wave repeatedly pulsed, we get from fig 14(c)

$$\delta_{n+1} = \delta_n + t_s - T \quad [4.12]$$

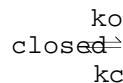
so dividing by  $\tau$

$$\theta_{n+1} = \theta_n + \Omega - g(\theta_n) \pmod{1}, \quad \Omega = t_s/\tau \quad [4.13]$$

where  $t_s$  is the interstimulus distance. Such cells display mode-locked beating and chaotic changes as  $t_s$  is varied.

Periodic stimulation of giant squid axons have similarly demonstrated mode-locking, bifurcation to chaos and the transmission of chaotic signals along the nerve axon. Spontaneous chaotic firing was also demonstrated in the mollusc *Onchidium* under synaptic blocking by  $Co^{2+}$  ions (Hayashi & Ishizuka 1986), and in simian motor neurons (Rapp et. al. 1985), and single cortical cells (Albano et. al. 1986a) establishing the involvement of chaos in individual neurons *in vivo*. Neuronal networks which involve the interaction of many resonant systems thus have a high probability of displaying chaotic dynamics through the quasi-periodicity route.

**(b) Fractal Dynamics in a Voltage-dependent  $K^+$  Ion Channel.** The traditional model for ion channel kinetics is that the channel has open & closed states, each of which has a rate constant



Given the cumulative probability  $P(t)$  that a channel will remain closed over  $[0,t]$ , we have

$$P(t+\Delta t) = P(t) [1 - k_0(t)\Delta t] \quad [4.14]$$

Hence 
$$\Delta P = P(t+\Delta t) - P(t) = P(t) [-k_0(t)\Delta t] \quad [4.15]$$

and so 
$$\frac{d \ln P}{P} = -k_0(t) dt, \text{ or } \frac{d \ln P}{dt} = -k_0(t) \quad [4.16]$$

Hence 
$$P(t) = e^{-\int k_0(t) dt} \quad [4.17]$$

In a Markov process  $k_0$  is constant as in fig 15a[1] and we get :  $P(t) = A.e^{-kt}$ . [4.18]

If we refine the Markov model to include further discrete states, such as closed-closed-open, we get two exponentials and a step curve for  $k_0(t)$  as in a[2]. If instead we look for a power law of  $t$  (Liebovitch et. al. 1987 a,b) :

$$k_0(t) = A t^{-D} \quad [4.19]$$

as in the fractal equation [1.16], the *log-log* plot will give a sloping line as in a[3], and  $P(t)$  can be calculated as an integral from [4.17] and [4.19]. The experimental plots in fig 15(b) show a fractal model gives the best fit for ion channels ( $D_c = 0.79$ ) in the corneal endothelium and also in hippocampal neurons ( $D_c = 1.07, D_o = 0.34$ ).

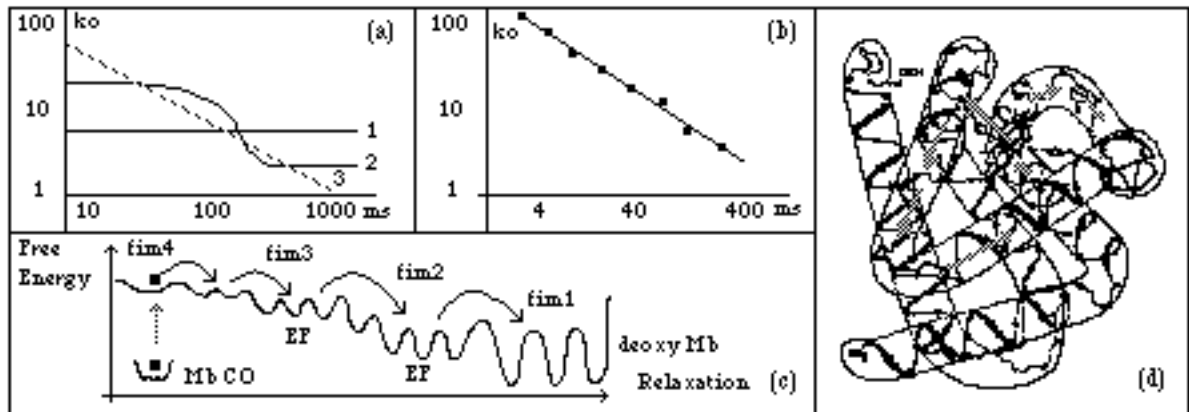


Fig 15 (a) Theoretical predictions of Markov & fractal ion channel models. Note the Markov models give horizontal or step functions, requiring an infinite number of states to represent the same effect as the fractal model sloping line.

(b) The  $K^+$  channel kinetics in a corneal endothelium cell, confirming conforms to the fractal model.

(c) Relaxation of excited myoglobin involves four functionally important motions and many equilibrium fluctuations illustrating the basis of the fractal model in diverse molecular excitations.

(d) The 3-D pathways of relaxation of the myoglobin molecule.

The significance of this can be best understood by looking at a better characterized system, photo-dissociation of CO-myoglobin (Ansari et. al. 1985). In fig 15(d) is shown the structure of myoglobin illustrating how a global conformational reaction occurs to the relaxation of the dissociated molecule. This relaxation involves a hierarchy of several *functionally important motions* (fim) each with several *equilibrium fluctuations* (EF) having varying potential barriers and rate constants. Relaxation thus involves many quantum interactions in which phonons, Davydov solitons, coherent and other excitations are exchanged. Various electronic orbital structures such as delocalized electrons, spin-orbit coupling, triplet-state electrons and dipole structures which could enable Bose condensation of coherent photons have been proposed in biomolecular systems which profoundly complicate this fractal structure. Frölich (1968,1975) has suggested that the cyto-skeleton and membrane may admit coherent states. The complexity of three-dimensional structure of a protein, resulting from the hierarchy of strong and weak bonding & water structures, and the many conformational changes possible make for a high-order of variation in state on many scales consistent with the fractal model. Aperiodicity in protein primary sequence also favors a cascade of distinct interactive quanta in tertiary structure. Such considerations apply alike to the proteins including enzymes, ion channels & microfilaments and also to the piezo-electric structure of the membrane.

## (5) Chaos and Chaotic Models in Neurosystems

### (a) The Freeman-Skarda model of the Olfactory Bulb

Although the general idea of chaos as a foundation for brain dynamics has been mentioned by several researchers over a considerable period (Nicolis 1983, 1986), the model of Skarda & Freeman (1987) is one of the most completely developed from both a theoretical and an experimental point of view. In this model, chaos is proposed as the basic form of collective neural activity for all perceptual processes, whose function is threefold : as a controlled source of noise, to access previously learned patterns and to learn new patterns. Although computer-based information processing concepts have been widely used in modelling peripheral and some central sensory systems, the specific structures of feature-detection and command neurons have not been successfully extended to the associative areas of the cortex. Skarda and Freeman comment "brains don't work in the way everyone including ourselves expected them to. The form in which sensory information is represented in the olfactory bulb is a spatial pattern of chaotic activity covering the entire bulb involving equally all the neurons in it and existing as a carrier wave or wave packet".

On inhalation, a transition occurs from low level chaos fig 16(f) to a trajectory which in the case of a familiar odor will settle into one of several periodic orbits, but in the case of a new odor will avoid existing periodic attractors, hunting chaotically until a new periodic attractor is established over time, forming both a new familiarized response and a new *symbol*. Inhalation thus causes a bifurcation of the dynamic into one of many periodic orbits for each learned odour, embedded in a chaotic regime. An unusual odor results in a low peak frequency and broad spectrum with excessive phase modulation. Similarly the work of Skinner et. al. (1989) has demonstrated that novel stimuli increase the correlation dimension in the bulb, while familiar stimuli reduce it. The dynamics proposed consists of

two modes. In the diastolic mode the bulb responds to input from afferent neurons - (broad spectrum states). In the systolic, the bulb goes into high-energy interactive bifurcation. This two-phase activity is remarkably similar to the two-phase activity of the ART architectures.

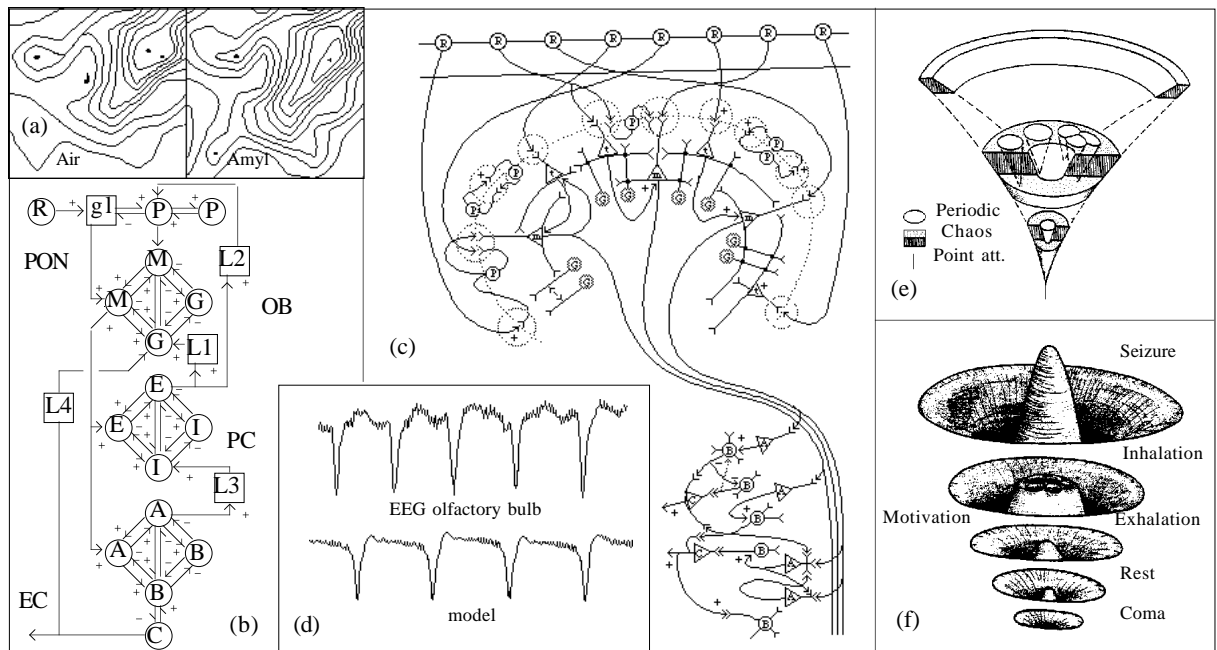


Fig 16 (a) 8x8 matrices of bulb response illustrating topological differences in excitation for air and amyl nitrate. (b) Modular nerve cell assembly, connecting the olfactory bulb, (OB) pyriform cortex (PC) and entorhinal cortex (EC) involves mutual inhibition (e.g. GG, II, BB) and broad feedback pathways (L3 etc.) (c) The realization of the above model circuit in a network of bulb cell types. (d) EEG in seizure in the bulb and model simulation, showing the dynamics of the model agrees with experiment. (e) Bifurcation diagram and (f) Phase portrait of the stages of chaotic excitation in the model.

The chaotic dynamic may provide a way of entraining neurons that is guaranteed not to lead to cyclic or spatially pre-structured activity, allows unbiased access to every limit cycle attractor, provides escape from established attractors under unfamiliar stimulus and ability to create new limit cycle. The response has extremes of seizure and coma representing a chaotic attractor and fixed attractor. The 'background' odor likewise consists of low amplitude chaotic activity, which on measurement gave a correlation between 4 & 7. The dynamic becomes latent during exhalation and in the absence of motivation. These ideas are illustrated in fig 16(e,f) .

An experimental program was carried out in which a conditioned odour stimulus CS elicited a conditioned response CR indicating discrimination ('licking' only in the case of CS+). A 3.5 x 3.5 mm 8 x 8 array of electrodes was implanted with a 2 msec sampling frequency. Filters were set at 10 and 160 Hz. A 76 msec sampling interval thus required 64 x 38 x 12 bits. The 64 traces were fitted by regression to 5 elementary basis functions, and a residual variance from the sum of these, and the high and low filter matrices were taken and tested for capacity to classify events correctly wrt CS and CR. Although the raw EEGs did not show obvious distinguishing characteristics, the first basis matrix was found to be an effective measure of discrimination, once occasional artifacts were removed. A sample amplitude matrix is illustrated in fig 16(a). Chaotic dynamics is likely to result from an interplay between the major neurotransmitter types such as GABA and nor-epinephrine underlying the specific classes of neuron.

A 4-module nerve cell assembly model is illustrated in single component form in fig 16(b). The (P)eriglomerular cells are excitatory to each other and to (M)itral cells. Inhibitory interneurons [(g)ranule etc.] are self-inhibitory and mutually excitatory among mitral cells in the bulb and pyramidal cells in pre-pyriform cortex. A more detailed neural circuitry for the bulb is shown in (c). A simulation of the NCA structure, based on second-order non-linear differential equations for each neuron was carried out by varying the excitatory gain between P and M. This resulted in a transition from quasi-periodicity to chaos and gave output similar in form to states of the EEG as in fig 16(d).

The overall dynamical nature of CNS processes may involve chaos as a fundamental component because resolution of one aspect of the dynamic into a stable attractor may result in destabilization of subsequent centres. For example convergence in the bulb may destabilize motor centres involved in the reaction to the stimulus. The stabilized behavioral motor action (licking) then leads to further input. The dynamics thus depends on constraints of self-organization through arousal and motivation. This results in time-dependent [non-stationary] dynamics in which attractors arise and decay through bifurcations. Furthermore, real behaviors display both multifunctionality of responses and the blending of several repertoires in a single behavior (Mptsos 1989). For example in the mollusc *Pleurobranchaea* feeding, exploration or regurgitation actions may be combined. This poses a serious problem both

for the experimentalist trying to establish a dimension from a time series and for the theorist attempting a description of the attractors or their resulting behavior. The nature of the dynamics may consist of a fractal domain in which attractors occur on differing time scales. The basis of an attractor is thus unlikely to lie in rigid anatomical structures, but in dynamical interaction. Chaos also involves structural instability as specific classes of neurons are brought to threshold and undergo an exponential response with depolarization.

Like the connectionist models of neural nets, the Skarda-Freeman model utilizes parallel distributed processes to lead to a self-organized optimization. However, most neural net models are digital or seek local minima and do not admit chaotic background states. The connectionist models do not generally involve the local feedback necessary to develop chaotic and limit cycle dynamics. For example the Hopfield net has point attractors and does not lend itself to dynamical refreshing. The inherent problems of entrapment at local minima in neural nets are handled in the Boltzman machine by stochastic annealing rather than chaos. Back propagation as a process is slow and dispersed in the brain.

A variety of possible functional roles have been suggested for chaotic processes :

- (1) they allow unbiased access to stable states, provide escape from stable states under unfamiliar stimulus and the ability to create new states.
- (2) they provide a basis for the development of symbols as the stable attractors of the dynamic from a more fundamental dynamical continuum. Thus while the models of artificial intelligence cannot fully represent chaos, dynamics may be able to represent symbol creation and manipulation.
- (3) they provide a natural spatially-global basis for developing self-organization through stability structures, similar to the role of protein tertiary structure in complementing the data storage of the genetic code. Physical systems such as turbulent fluids display formation of fractal dissipative bifurcations, which are a rich source of new structure. Chaotic variation may thus be a central route for developing new structures in the brain.
- (4) the need for random processes such as *annealing*, provides a basis for chaotic fluctuations to escape local minima in constrained optimizations.
- (5) they may enable a very efficient form of data compression in memory in which the complexity of a given CNS state is reduced to the topological form of key attractors. A similar role has been proposed for the filtering action of integrative attention.
- (6) they provide for a potentially indeterminate brain consistent with the roles of consciousness and free-will.

Critics of such models claim that it has not been demonstrated why chaos is essential to be able to carry out the tasks required in the bulb or C.N.S (Skarda & Freeman 1987). Other mechanisms such as the ART model, are cited as alternative explanations which can 'self-organize, stabilize, & scale a sensory recognition code in response to a list of binary input patterns'. The matrices in the experiment are claimed to represent more the state of motivation and the adaptive response than pattern recognition, despite being pre-sensory. Indeed relearning a previous odor after aversive conditioning results in a new pattern. However according to Freeman, adaptive resonance models based on mismatch detectors which stimulate arousal if match is insufficient, do not appear to have supporting structures in the neuronal architecture, because feedback from the pre-pyriform cortex to the bulb is not topographical. Nevertheless the obvious similarities between the functional two-phase modes of operation of each suggests compatibility of the theories. It is possible that further investigation of such systems will demonstrate a complementation of these two models in which plasticity in feature detection requires a continuous unstable dynamical version of the ART configuration in which dynamical chaos is identified with the sequential search phase.

#### **(b) Experimental Chaos in the Electroencephalogram**

The status of the EEG, despite for a time being eclipsed by that of single neuron recordings, has since become a classic area for investigation of chaotic dynamics at the neurosystems level. Although the EEG is described as periodic and a series of frequency regimes have been defined [ 1-3 Hz  $\delta$ , 4-7  $\gamma$ , 8-14  $\alpha$ , >14  $\beta$  ] (Lane 1986) its power spectrum has a broad band spread characteristic of filtered noise or chaos, fig 17(e). The source of the EEG remains obscure. Although it was initially proposed to arise from collective action potentials e.g. from pyramidal cells, the lack of correlation between single cell recordings and the EEG has led to two hypotheses, local variations in dendritic potentials and changes mediated by  $K^+$  transport in glial cells, as supported by data from electroretinograms (Galambos 1989). It may involve all of these in varying measure. Bullock (1989) stresses the importance of cooperativity in generating the micro-EEG over short time ( $10^{-1}$ s) and space (1 mm) intervals and the correlation between both unit spikes and graded potentials in a fair sample of the neural population.

The obscurity of the EEG raises the question as to whether it represents functional or maintenance activity, however the relation, firstly between the EEG and broad mental states, and secondly between evoked or event-related potentials (EPs or ERPs) and behavior support the relevance of the study of the EEG to the form of brain dynamics. ERPs such as the 'expectancy' wave & P300 (Hooper & Teresi 1986, Maurier 1989) are well-known. In fig 17(d), a smaller evoked potential amplitude occurs for a preceding higher amplitude EEG, and in 16(c) anticipated stimuli result in coherent EEGs (Basar et. al. 1989).

Once signal averagers made possible the extraction of evoked potentials, researchers such as Basar (1983a,1990) began to suggest the possibility of EEG fluctuations being a result of a strange attractor. Subsequently, Babloyantz

et. al. (1985,1986), Rapp (1985) and other researchers established low-dimensional attractors in Slow Wave Sleep, epilepsy and other brain states, fig 17(a) (Babloyantz 1989). The occurrence of low-dimensional attractors, in both pathological and natural states supports the involvement of chaos as a fundamental aspect of brain dynamics.

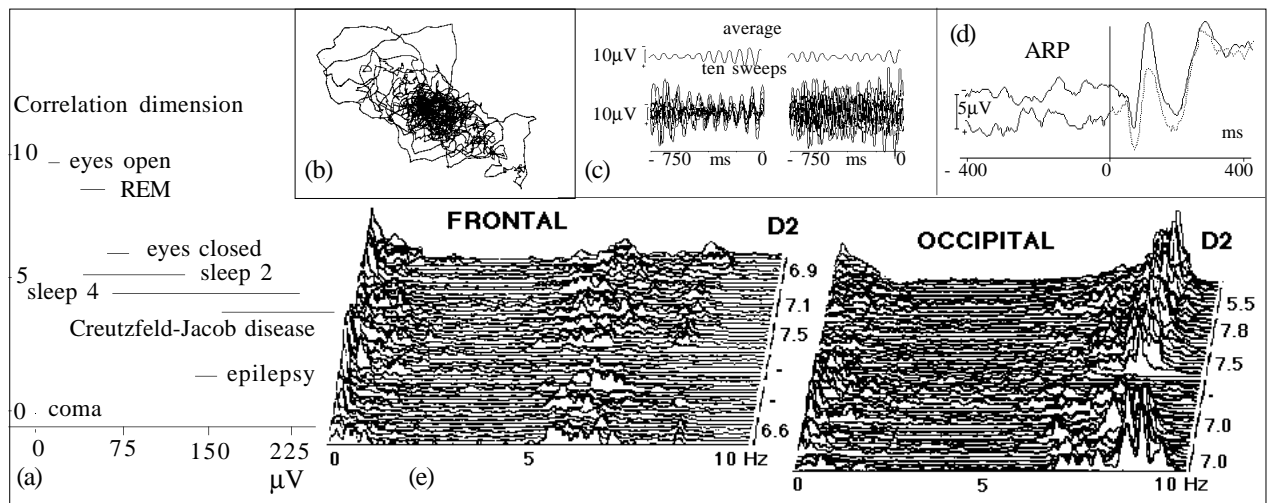


Fig 17 : (a) Typical correlation dimensions of a variety of natural and pathological brain states.

(b) A 2-D map of a chaotic attractor in stage 4 sleep

(c) Coherence of EEG recording in anticipated events and desynchronization in the absence of anticipation.

(d) Average Evoked Potential is reduced for a prior larger EEG

(e) Time-evolving 2-D power spectra of  $\alpha$ -rhythm, occipital and frontal showing variation with time in both the frequency spectrum and the correlation dimension as well as significant differences in the dimension between frontal and occipital dynamics.

The higher dimensionality of the active waking brain, fig 17(a), is consistent both with high-dimensional chaos and with filtered noise. Models have been proposed using coupled linear oscillations with noise (Wright 1989,1990) for reticular activation. The brain may in fact utilize all three modes : chaotic, periodic and stochastic. Some discrete forms of information processing for example could appear as noise. The activity of single neurons has been found to include both cells with activity indistinguishable from noise and also neurons displaying low dimensional chaos (Albano et. al. 1986a). The development better techniques for discriminating quasi-periodic noisy data from chaos in higher dimensions than 7 is essential before any detailed analysis can be made into the structure and variety of global neurosystems dynamics. However the status of chaos as an aspect of neurosystems dynamics appears well-confirmed.

Although the discovery of chaos has been identified with the lower dimensional states such as sleep and pathological states, higher dimensions do not contradict the existence of chaotic dynamics. It is thus wrong for researchers to conclude that chaos is only an attribute of the quiescent or malfunctioning brain. Thus low dimensions have sometimes been associated with a more maintenance-oriented activity and high dimensions with noise or varying information content. Very high dimensions consistent with noise or chaos could still result from complex chaotic dynamics with a vast number of interacting subsystems. Dimensions below 10 are particularly significant when the very large number of degrees of freedom in a system comprising  $10^{10}$  neurons and  $10^{15}$  synapses is considered, and high dimension or non-saturation may reflect multiple attractors rather than random activity *per se*, such as spontaneous background firing. The structural stability of periodic attractors make them insensitive to perturbations such as external stimuli. Chaotic dynamics is thus suggested as having a role of enabling varied response to stimuli, providing the capacity to adopt new states outside a fixed repertoire and providing for an increasing proportion of new information in the system in relation to the initial information - i.e. responsiveness.

Studies of the  $\alpha$ -rhythm illustrate the complexity inherent in studying chaos in the EEG. The correlation dimension varies from 8 down to between 3 & 5 depending on experimental techniques such as 5 - 15 Hz filtering. The dimension will vary both from time to time and from electrode to electrode, frontal areas often having high dimensional activity which does not reach saturation of embedding dimension and occipital areas having low dimensional chaos, for example with eyes closed. Individual local cells groups may or may not be either blocked by opening the eyes, driven by flicker or altered by specific mental tasks. It thus appears that specific strange attractors may be dynamically variable and subject to creation and destruction by bifurcations. Bullock has drawn attention to the fact that a well defined saturation plateau indicates high determinacy in the signal with low noise. However distinguishing dominating resonances such as the occipital  $\alpha$ -rhythm from less energetic components needs further analysis. Time-evolution of the power spectrum, fig 17(e) is one way of extending the analysis (Basar 1990). The variation of waveform with brain area and overall change in correlation dimension over time are both evident.

Several experiments support event-related desynchronization of  $\alpha$  activity. In Basar et. al. (1989), anticipation of a repetitious omission of a regular stimulus showed coherence in EEG between successive sweeps, while lack of certainty induced by random omissions resulted in desynchronized waves, fig 17(c). Hoke et. al. (1989) using

magnetoencephalography demonstrate elegantly the development of coherence in the event-related MEG upon the occurrence of a repeated signal. In fig 18(a) is shown the development of two regions of coherent phase. Independence of variation of mean amplitude from phase changes in some of these steps indicates distinct mechanisms may be involved. These results further support the idea of the chaotic epochs in a dynamic being the ones in which sensitivity to changing input occurs.

Higher frequency activity has also reported, including 40 - 60 Hz oscillations (Basar et. al. 1989). Evidence supporting coherence at these frequencies between functional columns has been found in the visual cortex, suggesting that resonances rather than specific neuronal architecture may be the substrate for specific perceptual events. Even higher frequency activity 100-1000 Hz occurs in the cerebellum and brain stem centres. Major resonances, such as  $\alpha$  and  $\theta$ , may thus result from resonances in the connection of cortical, thalamic and brain stem centres, despite the pacemaking periodicities e.g. of  $\alpha$  apparently being driven by the thalamic nuclei.

The existence of dominant frequency bands supports the notion that there exist periodic oscillations or predominant low-dimensional attractors with intermittent resonance, which maintain coherence in neural networks. Note from fig 2(a) that chaotic systems can also have dominant bands. Intermittency may be essential to avoid resonances preventing responsiveness or even reaching seizure. Resonance between lower level neurons activated by the same stimulus would enhance the input to appropriate higher-level cells. If the resonant frequency of a cell varies with its hyper- or de-polarization, cell populations will enter or leave the resonance depending on their synaptic input state. Models have been developed for major oscillations based on time-dependent coupled linear oscillators. These do not however model the chaotic feedback aspects of dynamics.

Other models based on chaotic oscillators which intermittently excite specific neuron sub-assemblies have also been proposed. These highlight another very different possible role for chaos, the compression of input data (Nicolis 1983,1986), Skinner et. al. (1989)). A governing attractor system which forms a dynamic model of the input, contains far less data than required to describe all the dynamical states, including their fractal boundaries and hence permits a very significant data compression. Such mechanisms also provide a role for suppression of familiar input (e.g. in the thalamic  $\alpha$ -oscillator), selective attention having the function of simulating only the unfamiliar and hence non-simulated aspects of stimuli. This mechanism is also reminiscent of ART. Note that chaotic PLMIs may also form periodic nets (Labos 1986).

The dynamical model requires development of a scheme which possesses modulated resonances or modulated coupling between cells or cell-assemblies in the layered neuronal network. A basis for such a *threshold-feedback* model is a layered net in which the internal feedback is modulated by altering the threshold of the interneurons responsible for maintaining the feedback between cells within a layer. As the mode moves from systole to diastole a change in these thresholds would convert the layer from positive or neutral (linear) coupling, similar to a stable laser, to unstable equilibrium through mutual negative feedback, resulting in structural instability and generalized competitive bifurcation, or to asymmetric feedback permitting limit cycles and chaos. On a modular scale this could direct selective attention to unresolved features. The circuit of fig 16(b) has elements of this structure through the feedback between the 4 modules and the excitation and inhibition within the net of a single module. A key element in the model is identifying the synapses mediating the threshold change responsible for mode change. The major cortico-thalamic-basal resonances mediating arousal in the CNS could thus be based on the modulations which hold the stable attractors, but systematically perturb the fractal regions of chaos until a major attracting system emerges, forming a dynamical version of ART.

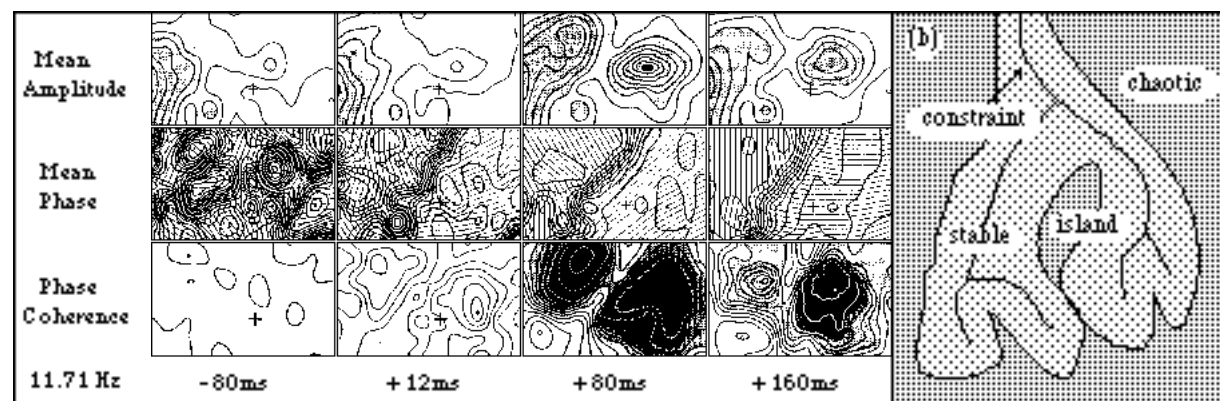


Fig 18 : (a) Spatial coherence in an Event-related Potential (Hoke et. al. 1989), (b) Chaotic model of cognition.

A model for cognition involving chaos fig 18(b) applies similar principles. Incoming sensory information is coded in the form of a variety of structural transforms of the input representing aspects such as line-orientation, colour, tone, through to abstractions such as the 'grandmother' concept. These would arise as dynamical stability structures. Those aspects of a given problem which are consistent with the input constraints would attain coherence in their modules, extending the form of the input constraints leaving a complementary chaotic domain with a fractal

boundary. The evolution of this system into a stable global regime, constitutes the solution to the problem. If however the dynamic retains chaotic islands which cannot be resolved from the boundary constraints, the problem remains incompletely solved, possibly requiring major reconstruction of the attractors and their surrounding stable regions - i.e. reformulation of the approach.

## **(6) The Fractal Extension of Chaos to the Quantum Level**

The discovery that fractal and chaotic dynamics plays a significant role in processes from the neurosystems level, down through the cellular and synaptic levels to the ion channel at the molecular level raises important new issues concerning the relationship between sensitive dependence and causal descriptions of neuronal dynamics. It becomes natural to ask the question "At what level does the fractal dynamics actually stop subdividing?"

In particular, since mutual interdependence can exist between unstable neurons and global neurosystems instabilities, the possibility of fluctuations at the molecular level, the quantal level of vesicles, or in the membrane being linked to global changes requires further examination. Usually nervous systems are believed to be subject to the laws of mass action and are treated as causal mechanisms which are not subject to quantum or other random fluctuations. Part of the reason for this is to ensure computing networks are *robust* to the kind of local damage which is seen to occur physiologically during the life of a nervous system. In particular, during the life of a human 100,000 cells may be lost a day, accumulating during a lifetime to around 10% of all cells in the central nervous system. Obviously brain function must have significant stability built in, which makes the system robust to such vagaries.

Nevertheless the extension of the notion of robustness to all aspects of central nervous function may be a serious conceptual error, which fails to take into account the need for sensitive dependence and structural instability, to guarantee tuning of the system to arbitrarily subtle external stimuli, and to permit the development of new internal models, not provided by the structure of the circuitry at a given point in time as stability structures. Sensitive dependence of chaotic neurosystem dynamics may thus provide a mechanism in which fluctuations at the cellular, synaptic and ultimately the molecular level may become linked, so that fluctuations resulting from quantum uncertainty could become amplified to the global level. Mandel (1986) illustrates a similar hierarchical route in discussing the effects of lithium.

The nature of instabilities in chaotic systems requires only a small sub-population of cells to be in an unstable state. Such instabilities can easily be restricted to short-term dynamical characteristics which preserve long-term robustness. A *holographic* transform-based memory is naturally robust to partial loss of information, because cell loss or disturbance results only in a differential loss of discrimination of all stored items, and thus does not require microsystem robustness. Thus the possibility remains open that fluctuations at the cellular or even molecular level may play a part in resolving global instabilities through sensitive dependence.

We will examine these possibilities on each level of organization :

**(a) Neurosystems:** Sensitivity to initial conditions makes it possible for one or a few critical neurons to alter the stability of a much larger neurosystem of stable cells. Given a structurally unstable neurosystem which is about to undergo bifurcation, only a very small sub-population of critical cells need be in an unstable state to determine the stability-breaking of the global dynamic. However the crossing of threshold of such a critical neuron could conversely develop in a time-dependent cascade into a global bifurcation of a whole net. In principle this would make the neurosystems level sensitive to fluctuations at the level of a single neuron.

**(b) The Neuron:** A neuron whose threshold is tuned to its input level acts as an unstable bifurcator of a fluctuating input state. The occurrence of chaotic dynamics in single neurons and the use of mutual inhibition and threshold tuning in biological and neurosystems architecture provide a further basis for instability through sensitive dependence. The occurrence, for example in the hippocampus, of neurons receiving simultaneous input via distinct neurotransmitters from a variety of sense modes the reticular activating system and other sources supports mutual functional mapping between global neuro-dynamics and that of single neurons, which would enable single cell or micro-system instabilities to become global. The combination of unstable bifurcator cells and those with chaotic dynamics would provide a powerful means for amplification of such neuronal instabilities.

**(c) The Synapse:** The synapse is capable of both discrete and continuous transformation of the input into output. In cortical synapses, there is no need for the large number of vesicles in the neuro-muscular junction and it has been proposed that in some synapses, the release of contents of a single vesicle is sufficient to traverse the threshold and elicit a post-synaptic response. Even in the standard model the release of the acetyl-choline in a single vesicle, causes discrete micro-potentials which depolarize the membrane by about 1 mV, sufficient to result in an action potential if a cell is already at threshold.

**(d) The vesicle:** The vesicular structure in a sense results in the amplification of quantal instabilities from the level of the molecule to the larger level of the vesicle through the agency of the topological closure of membrane structure. The nature of vesicle exocytosis, involving about 10,000 neurotransmitter molecules and 2000 ion channels, generally appears to create a large enough population to produce causal mass action at the neuro-transmitter level. However the kinetics of vesicle association with the pre-synaptic membrane is determined by binding to one, or a few proteins, making vesicle release a function of the kinetics of one or a few molecules. The precise mechanism of vesicle exocytosis is not yet elucidated, but may involve binding to the membrane protein synapsin I.

A quantum-kinetic model would be particularly relevant in excitation requiring only one or a few vesicles. Eddington (1935) and Eccles (1970) have raised the possibility of quantum-mechanical action of the vesicle and noted that the uncertainty of position of a vesicle of  $400 \text{ \AA}$  diameter and mass  $3 \times 10^{-17} \text{ g}$  is about  $30 \text{ \AA}$ , comparable with the thickness of the membrane, making neurotransmitter release potentially subject to quantum uncertainty.

**(d) The ion-channel:** Activation of a single ion channel requires one or two neurotransmitter molecules. While the ion flux resulting from a single open ion channel will not generally elicit an action potential, if the channel happens to command a critical site on the two-dimensional dendritic surface, for example close to the cell body where the action potential begins, and the cell is at or near threshold, then the single quantal encounter of a neurotransmitter binding to an ion channel could evoke an action potential.

*Sensitive dependence* and *quantum amplification* could thus act together to make the brain potentially able to detect fluctuation at the quantum level. This is consistent with the sensitivity of sensory apparatus which are all capable of detections at or close to the level of single quanta. For example the minimum number of photons required to elicit a response in a nocturnal animal, or the number of pheromone molecules required to elicit behavioral reaction in moths, are both close to unity.

The possibility of a connection between quantum mechanics and brain function has been a source of interest since the discovery of the uncertainty principle, partly because of its implications for consciousness & free-will. The connection between the observer's mind and quantum mechanics is pivotal in some interpretations of wave function collapse. Bohm's work on the Einstein-Podolsky-Rosen conjecture, Bell's theorem and the Aspect experiments (Clauser & Shimony 1978, Aspect 1982) which display spin-correlations between a split photon pair over space-like intervals have demonstrated that hidden variable theories must be non-local, leading several researchers to postulate the idea of non-local states correlating the activity of various parts of the brain (Penrose 1987). Collapse of the wave function appears to be the aspect of quantum mechanics which best supports the sensitivity and indeterminacy of chaotic systems, since the evolution of the quantum Hamiltonian appears to avoid true chaos. Popper and Eccles (1977) and Margenau (1984) have also discussed the possibility of quantum reduction being associated with the nature of free-will and the mind. Basar (1983b) has suggested matrix theory and Feynman diagram approaches (Stowell et. al. 1989) to resonances at the neurosystems level by drawing from ideas in physics in brain modelling.

However it is one thing to suggest that quantum fluctuations could in principle evoke global bifurcations of brain function, but quite another to determine what advantage might accrue from such seemingly stochastic activity. We will thus examine models which attempt to explain possible advantages of quantum uncertainty in brain function.

Deutch (1985) has analysed the potentialities of a quantum computer which has a 'fuzzy' logic representing quantum superpositions of states to form a probability function in the interval  $[0,1]$  in place of the usual  $\{0,1\} = \{T,F\}$  of formal logic. Although the algorithmic capacity of such a quantum computer does not extend the class of functions computable by a conventional Turing machine, several specific instances have been given in which a quantum computer might solve special tasks more efficiently, (Lockwood 1989). However these do not appear to provide significant advantages over parallel distributed processing. Both these authors adhere to the Everett many-worlds interpretation of quantum mechanics in which the collapse of the wave function never occurs, and all histories having a non-zero probability under the quantum prediction are presumed to co-exist as parallel aspects of a cosmic wave function. This places a specific limit on their capacity to utilize wave function collapse, and restricts their models to the use of superpositions of quantum states in place of a single physical state.

The mathematician Roger Penrose (1986,1989) has also studied the relation between the conscious brain and quantum physics in depth and attempted to combine quantum theoretic and relativistic ideas. He has suggested that collapse of the wave function may be a deterministic process based on the interaction of the superimposed wave function with the gravitational field at the level of one graviton. Gravity is the most difficult force to integrate into a quantum approach. The development of superstring theories and higher dimensional Kaluza-Klein space-times may establish a consistent theory of quantum gravity, making this suggestion open to more rigorous evaluation.

The dual-time model (King 1989), which combines quantum theory and special relativity, develops a *supercausal* theory which is consistent with conventional quantum mechanics, but allows for correlations between reduction events over both space and time. This replaces the stochasticity of the quantum model with a time-symmetric description, based on the *transactional interpretation* of quantum mechanics in which an exchanged particle is treated as a transaction between emitter and absorber. Because the boundary conditions of a transactional exchange necessarily include future states of a system, the initial conditions remain insufficient to fully determine the system implying that future states of a system influence reduction events by forming part of the boundary conditions. In systems in which only one or a few reductions take place for each state, convergence to the quantum probability interpretation does not occur. Such conditions arise when fluctuations lead to a sequence of new states, as is the case when they result in successive bifurcations of the dynamic. A system exchanging a restricted set of particles internally or externally might then gain access to a form of predictivity which could explain the evolutionary emergence of consciousness and free will as consequences of such *causally indeterminate* aspects of brain function.

The model thus proposes that what may appear to be quantum noise to an external observer may enable a form of

predictivity to be utilized by transform processes in the generation of an internal space-time model. It should be noted the the global architecture of the pre-frontal cortex and limbic system (Alkon 1989, Mishkin & Appenzeller 1988) could be closely described as a *holographic representation of time* in which future and past states are both represented using transform features similar to those of the auditory and visual sensory processing. While memory represents past states, the orientation of organized goal-seeking behavior implicitly involves future states. Prefrontal lobotomies in both man and monkeys are known to effect *both* these processes (Alkon 1989).

Conscious awareness would in this perspective be identifiable with the quantum indeterminacy of major chaotic resonances involving the cortex, mid-brain and limbic system as exemplified in the EEG. It is also possible that the subjective sensory aspects of mind, including the qualitative differences between the senses as exemplified by *colour, sound, odour* and *touch* arise from the different ways these modes of stimulation act at the *quantum* level, as *photon, phonon, orbital interaction* and *soliton* rather than from a merely structural difference in feature detectors. Our 'internal model' may thus act by re-evoking such quantum transformations in the brain.

The development of chaotic excitations may have arisen in the earliest cells as a form of extra-cellular sense organ utilizing sensitive dependence. Electrochemistry has been proposed as a predecessor to genetic translation which may have emerged spontaneously as a stability structure in the 'RNA-era' (King 1978, 1990) before the development of coded enzymes, as a result of non-enzymic photo-electric ion transport. The ancient origin of molecules such as the amine neurotransmitters, and the components of phospholipids is notable in this respect. It is thus possible that electrochemical amplification of quantum chaos is a physical property fundamental to all eucaryote cells, providing a unique window on fundamental properties of quantum physics, which could be of cosmological generality.

**Summary :** The chaotic aspects of brain structure and dynamics have been discussed. The relation of chaos to fractal processes in the brain from the neurosystems level down to the molecule has been explored. It is found that chaos appears to play an integral, though not necessarily exclusive role in function at all levels of organization from the neurosystems to the molecular and quantum levels. An interesting consequence involving the possible interface between chaotic dynamics and quantum physics has been discussed because of its potential significance in resolving several of the most intractable conceptual problems to do with computability, the brain and the mind (Blakemore & Greenfield 1987, Hooper & Teresi 1987, Rose 1973, Searle 1979, Penrose 1986, 1989).

#### REFERENCES

- Albano A.M., Abraham N., de Guzman G., Tarroja M., Bandy D., Gioggia R., Rapp P.E., Zimmerman I., Greenbaum N., Bashore T., (1986a), *Lasers and brains : Complex systems with low-dimensional attractors*, in *Dimensions & Entropies in Chaotic Systems* Ed. Mayer-Kress G. Springer-Verlag, Berlin 231-240.
- Albano A.M., Mees A., de Guzman G., Rapp P.E., (1986b), *Data requirements for reliable estimate of correlation dimensions* in *Chaos in Biological Systems* ed. Degn H., Holden A., V., Olsen L.F. , Plenum Press, New York, 207-220.
- Albano A.M., Muench J., Schwartz C., Mees A., Rapp P., (1988), *Singular-value decomposition and the Grassberger-Procaccia algorithm*, *Phys. Rev. A* **38** 3017-3026.
- Alkon D.L., (1989), *Memory storage and neural systems*, *Scientific American*, **July**, 26 - 34.
- Ansari A, Berendzen J., Bowne S., Frauenfelder H., Iben I., Sauke T., Shyamsunder E., Young R., (1985), *Protein states and protein quakes*, *Proc. Nat. Acad. Sci.* **82** 5000-4.
- Aspect A., Dalibard J., Roger G., (1982), *Experimental tests of Bell's theorem using time-varying analysers*, *Phys. Rev. Lett.* **49**, 1804.
- Auerbach D, Procaccia I., (1990), *Grammatical complexity of strange sets*, *Phys. Rev. A* **41**, 6602-6614.
- Babloyantz A., (1989), *Estimation of correlation dimensions from single and multichannel recordings*, in Basar E., Bullock T.H. eds. *Brain Dynamics* Springer-Verlag, 122-130.
- Babloyantz A. & Salazar J.M., (1985), *Evolution of chaotic dynamics of brain activity during the sleep cycle*, *Phys. Lett.* **111A**, 152 - 156.
- Babloyantz A. & Destexhe A., (1986), *Low-dimensional chaos in an instance of epilepsy*, *Proc. Nat. Acad. Sci.* **83**, 3513 - 3517.
- Barnsley M. (1988) *Fractals Everywhere* Academic Press, New York.
- Basar E., (1983a), *Synergetics of neural populations : A survey of experiments*, in Basar E., Flohr H., Haken H. Mandell A.J., *Synergetics of the Brain* Springer-Verlag Berlin, Heidelberg, 183-200.
- Basar E., (1983b), *Towards a physical approach to integrative physiology I Brain dynamics and physical causality* *Am. J. Physiol.* **245**, R510-R533.
- Basar E., (1990), *Chaotic dynamics and resonance phenomena in brain function : Progress, perspectives and thoughts*, in Basar E. ed. *Chaos in Brain Function* Springer-Verlag, Heidelberg 1-30.
- Basar E., Basar-Eroglu J., Röschke J., Schütt A., (1989), *The EEG is a quasi-deterministic signal anticipating sensory-cognitive tasks*, in Basar E., Bullock T.H. eds. *Brain Dynamics* Springer-Verlag, 43-71.
- Bern M. & Graham R., (1989), *The shortest network problem*, *Sci. Am.* **Jan**, 66 - 71.
- Blakemore C., Greenfield S., (1987), *Mindwaves*, Basil Blackwell, Oxford.
- Bullock T.H., (1989), *The micro-EEG represents varied degrees of cooperativity among wide-band generators*, in Basar E., Bullock T.H. eds. *Brain Dynamics*, Springer-Verlag, 5-12.
- Butcher J.C. (1987) *The Numerical Solution of Ordinary Differential Equations*, Wiley, Chichester.
- Carpenter G.A. & Grossberg S., (1987), *ART2 Self-Organization of Stable Category Recognition Codes for*

- Analog Input Patterns* *Applied Optics* **Dec 1**, 4919 - 30.
- Casati G., Chirikov B., Guarneri G., Shepelyanski D., (1986), *Dynamical stability of quantum chaotic motion in a hydrogen atom*, *Phys. Rev. Lett.*, **56/23**, 2437-40.
- Chay T.R., Rinzel J. (1985), *Bursting, beating and chaos in an excitable membrane model*, *Biophys. J.* **47**, 357-366.
- Churchland P.M., Churchland P.S., (1990), *Could a Machine Think?*, *Sci. Am.* **Jan.** 26-31.
- Clauser J.F., Shimony A., (1978), *Bell's theorem : experimental tests and implications*, *Rep. Prog. Phys.* **41**, 1881 - 1927.
- Cooper J.R., Bloom F.E., Roth R.H., (1982), *The Biochemical Basis of Neuropharmacology*, 4th ed. Oxford Univ. Pr.
- Cowan J.D., Sharp D.H., (1988), *Neural nets*, *Quart. Rev. Biophys.* **21** 365 - 427.
- Cramer J.G., (1986), *The transactional interpretation of quantum mechanics*, *Rev. Mod. Phys.* **58**, 647 - 687.
- Crick F., (1982), *Do dendritic spines twitch?* *Trends in Neuroscience*, **5**, 44-46.
- Crick F., Marr D., Poggio T., (1988), *An information-processing approach to understanding the visual cortex*, in *Brain Theory*, ed. Shaw G., Palm G. World Scientific, Singapore, 726-754.
- Darnell J., Lodish H., Baltimore D., *Molecular Cell Biology*, Scientific American Books 1986.
- Deutsch D., (1985), *Quantum theory, the Church-Turing principle and the universal quantum computer*, *Proc. Roy. Soc. Lond.* **A400**, 97-117.
- Devaney R.L. (1986) *An Introduction to Chaotic Dynamical Systems* Benjamin/Cummings, Menlo Park, CA.
- Devaney R.L., (1988), *Dynamics of simple maps*, in Devaney R.L., Keen L. ed. *Chaos and Fractals*, Proc. Symp. App. Math. A.M.S.
- Eccles J.C. ed., (1966), *The Brain and Conscious Experience*, Springer-Verlag, Berlin.
- Eccles J.C., (1970), *Facing Reality*, Springer, New York, Heidelberg.
- Eddington A.S., (1935), *New Pathways in Science*, Cambridge Univ. Press, Cambridge.
- Elliot D. & Ramomohan Rao K., (1982), *Fast Transforms : Algorithms, Analyses, Applications*, Academic Press.
- Freeman W., (1983), *Dynamics of image-formation using nerve cell assemblies*, in Basar E., Flohr H., Haken H. Mandell A.J. *Synergetics of the Brain* Springer-Verlag Berlin, Heidelberg 102-121.
- Freeman W.J. (1991) *The physiology of perception* *Sci. Am.* **Feb.** 34 - 41.
- Frölich H., (1968), *Long-range coherence and energy storage in biological systems*, *Int. J. Quant. Chem.* **11**, 641-649.
- Frölich H., (1975), *The extraordinary dielectric properties of biological materials and the action of enzymes* *Proc. Nat. Acad. Sci.* **72**, 4211-5.
- Galambos R., (1989), *Electrogenesis of evoked potentials*, in Basar E., Bullock T.H. eds. *Brain Dynamics*, Springer-Verlag, 13-25.
- Giesel T., Radons G., Rubner J., (1989), *Kolmogorov, d'Arnold, Moser barriers in quantum dynamics of chaotic systems*, *Phys. Rev. Lett.* **57/23**, 2883.
- Goldbeter A., Mattiel J., (1986), *Periodic behavior and chaos in the mechanism of intercellular communication governing aggregation of Dictyostelium amoebae*, in *Chaos in Biological Systems*, ed. Degn H., Holden A.,V., Olsen L.F. Plenum Press, New York, 79-90.
- Grassberger P., Procaccia I., (1983), *Measuring the strangeness of strange attractors*, *Physics* **9D**, 189-208.
- Grossberg S. (1983), *Neural substrates of binocular form perception*, in Basar E., Flohr H., Haken H. Mandell A.J. *Synergetics of the Brain*, Springer-Verlag Berlin, Heidelberg, 274-296.
- Grossberg S., (1987), *The Adaptive Brain* Vol 1 & 2, Elsevier / North - Holland, Amsterdam, 239 - 286.
- Grossberg S., (1988), *Neural Networks and Natural Intelligence*, M.I.T. Press, Cambridge, Mass. 251 - 315.
- Hayashi H., Ishizuka S., (1986), *Chaos in molluscan neuron*, in *Chaos in Biological Systems*, ed. Degn H., Holden A.,V., Olsen L.F. Plenum Press, New York, 157-166.
- Hayashi H., Nakao M., Hirakawa K., (1982), *Chaos in the self-sustained oscillation of an excitable biological membrane under sinusoidal stimulation*, *Phys. Lett.* **88A/5**, 265-266.
- Hodgkin A.L., Huxley A.F., (1952), *A quantitative description of membrane current and its application to conduction and excitation in nerve*, *J. Physiol.* **117**, 500-544.
- Hoke M., Lehnertz K., Pantev C., Lütkenhöner B., (1989), *Spatiotemporal aspects of synergetic processes in the auditory cortex as revealed by the magnetoencephalogram*, in Basar E., Bullock T.H. eds. *Brain Dynamics*, Springer-Verlag, 84-108.
- Holmes P.J., (1988), *Non-linear oscillations and the Smale horseshoe map*, in Devaney R.L., Keen L. ed. *Chaos and Fractals*, Proc. Symp. App. Math. A.M.S.
- Hooper J. & Teresi D., (1986), *The Three-Pound Universe*, MacMillan New York .
- Hopfield J., Tank D., (1986), *Computing with neural circuits : A model*, *Science* **233**, 626-633.
- Hubel D. & Wiesel T., (1979), *Brain mechanisms of vision*, in Flannagan D. ed., *The Brain*, Scientific American Books, Freeman, ISBN 0-7167-1150-8, 84 - 96.
- Jack J.J., Noble D., Tsien R., (1975), *Electric Current Flow in Excitable Cells*, Clarendon Press, Oxford.
- Kalil R.E., (1989), *Synapse formation in the developing brain*, *Sci. Am.* **Dec.** 76-85.
- Kandel E.R., (1979), *Small systems of neurons*, in Flannagan D. ed., *The Brain*, Scientific American Books, Freeman ISBN 0-7167-1150-8, 28 - 38.
- Kimmelberg H., Norenberg M., (1989) *Astrocytes*, *Sci. Am.* April 44-53.
- King C.C., (1978), *Unified field theories and the origin of life*, *Univ. Auck. Math. Rept. Ser.* 134.
- King C.C., (1989), *Dual-time supercausality*, *Phys. Essays* **2**, 128 - 151.

- King C.C., (1990), *Did Membrane Electrochemistry Precede Translation? Origins of Life & Evolution of the Biosphere* **20**, 15 - 25.
- Lane S.P., Mayer-Kress G., Holzfuß J. (1986), *Problems associated with dimensional analysis of electroencephalogram data*, in *Dimensions & Entropies in Chaotic Systems*, Ed. Mayer-Kress G., Springer-Verlag, Berlin, 246-256.
- Labos E., (1986), *Chaos and Neural Networks*, in *Chaos in Biological Systems*, ed. Degn H., Holden A.,V., Olsen L.F. Plenum Press, New York, 195-206.
- Li T.Y., Yorke J.A., (1975), *Period three implies chaos*, Am. Math. Mon. **82**, 985.
- Libet B., Wright E., Feinstein B., Pearl D., (1979), *Subjective referral of the time for a sensory conscious experience*, Brain **102**, 193 - 224.
- Liebovitch L.S., Fischbarg J., Konairek J.P., Todorova I., Wang Mei, (1987), *Fractal model of ion-channel kinetics*, Biochim. Biophys. Acta **896**, 173-180.
- Liebovitch L.S., Sullivan J.M., (1987), *Fractal analysis of a voltage-dependent potassium channel from cultured mouse hippocampal neurons*, Biophys. J. **52**, 979-988.
- Lockwood M., (1989), *Mind, Brain & the Quantum*, Basil Blackwell, Oxford.
- Mandell A., (1986), *Strange stability in hierarchially-coupled neuropsychobiological systems*, in *Dimensions & Entropies in Chaotic Systems*, Ed. Mayer-Kress G. Springer-Verlag, Berlin.
- Margenau H., (1984), *The Miracle of Existence*, Ox Bow Press, Woolbridge, Conn.
- Markus M., Kuschnitz D., Hess B., (1985), *Properties of strange attractors in yeast glycolysis*, Biophys Chem **22**, 95-105.
- Marr D., (1969), *A theory of the cerebellar cortex*, Jour. Physiol. **202**, 437-470.
- Maurier K., (1989), *The clinical use of P300 cartography in diseases with disturbed cognitive processing of the brain*, in Basar E., Bullock T.H. eds. *Brain Dynamics*, Springer-Verlag, 420-428.
- Matsumoto G, Takahashi N, Hanyu Y., (1986), *Chaos, phase-locking and bifurcation in normal squid axons*, in *Chaos in Biological Systems*, ed. Degn H., Holden A.,V., Olsen L.F. Plenum Press, New York, 143-156.
- Mees A., Rapp P., Jennings L., (1987), *Singular-value decomposition and embedding dimension*, Phys. Rev. A **36** 340-346.
- Mishkin M. & Appenzeller T., (1987) *The anatomy of memory*, Sci. Am. **June**, 62 - 71.
- Mpitsos G.J., (1989), *Chaos in brain function and the problem of non-stationarity*, in Basar E., Bullock T.H. eds. *Brain Dynamics* Springer-Verlag, 521-536.
- Mueller P. & Rudin D.O., (1968), *Action potentials in bilayer lipid membranes*, Nature **217**, 713 - 719.
- Nicolis J.S., (1983), *The role of chaos in reliable information processing*, in Basar E., Flohr H., Haken H. Mandell A.J. *Synergetics of the Brain* Springer-Verlag Berlin, Heidelberg 102-121.
- Nicolis J.S., (1986), *Chaotic dynamics in biological information processing : A heuristic outline*, in *Chaos in Biological Systems* ed. Degn H., Holden A.,V., Olsen L.F. Plenum Press, New York, 221-232.
- Nottebohm F., (1989), *From bird song to neurogenesis*, Sci. Am. **Feb.**, 56 - 61.
- Peitgen H.O. & Richter P.H., (1986), *The Beauty of Fractals* Springer-Verlag, Berlin.
- Penrose R., (1987), *Minds, machines & mathematics*, in Blakemore C., Greenfield S., *Mindwaves* Basil Blackwell, Oxford.
- Penrose R., (1989), *The Emperor's New Mind*, Oxford University Press.
- Penrose R., Isham C., (1986), *Quantum Concepts in Space & Time*, Oxford University Press.
- Pique J.P., Chen Y., Field R.W., Kinsey J.L., (1987), *Chaos and dynamics on 0.5 - 300 ps time scales in vibrationally excited acetylene*, Phys. Rev. Lett., **58/5**, 475-8.
- Pool R., (1989), *Quantum chaos : Enigma wrapped in a mystery*, Science **243**, 893.
- Popper K.R. & Eccles J.C., (1977) *The Self and Its Brain*, Springer Int. Berlin, Heidelberg, New York, London.
- Rapp P.E., Bashore T., Martinerie J., Albano A., Zimmerman I., Mees A., (1989), *Dynamics of Brain Electrical Activity*, Brain Topography **2** 99-118.
- Rapp P.E., Zimmerman I., Albano A., de Guzman G., Greenbaun N., (1985), *Dynamics of spontaneous neural activity in the simian motor cortex : The dimension of chaotic neurons*, Phys. Lett. **110 A(6)**, 335.
- Rasmussen H., (1989), *The cycling of calcium as an extracellular messenger*, Sci. Am. **Oct.**, 44-51.
- Röschke J., Basar E. (1989) *Correlation dimensions in various parts of the cat and human brain in different states*, in Basar E., Bullock T.H. eds. *Brain Dynamics* Springer-Verlag, 131-148.
- Rössler O.E., (1979), *An equation for hyperchaos*, Phys. Lett. **71A**, 155-157.
- Rössler O.E., Klein M., Hudson J.L., Wais R., (1988), in Kelso J., Mandell A., Schlesinger M. eds. *Dynamic Patterns in Complex Systems*, World Scientific, Singapore.
- Rose S., (1973), *The Conscious Brain*, Weidenfeld & Nicholson, London.
- Sander M., (1987), *Fractal growth*, Sci. Am. **Jan.** 82-88.
- Schierwagen A.K., (1986) *Dendritic branching patterns*, in *Chaos in Biological Systems* ed. Degn H., Holden A.,V., Olsen L.F. Plenum Press, New York, 191-193.
- Schroeder M.R., (1986), *Number Theory in Science and Communication* Springer-Verlag, Berlin.
- Schuster H.J., (1986), *Deterministic Chaos*, Springer-Verlag.
- Searle R.J., (1979), *Brain and Mind* Excerpta Medica Amsterdam.
- Searle R.J., (1987), *Minds and brains without programs*, in Blakemore C., Greenfield S., *Mindwaves* Basil Blackwell, Oxford.
- Searle R.J., (1990) *Is the brain's mind a computer program?* Sci. Am. **Jan.** 20-25.

- Skarda C.J., Freeman W.J., (1987), *How brains make chaos in order to make sense of the world*, Behavioral & Brain Sciences **10**, 161-195.
- Skinner J.E., Martin J., Landisman C., Mommer M., Fulton K., Mitra M. Burton W., Saltzberg B., (1989), *Chaotic attractors in a model of neocortex : dimensionalities of olfactory bulb surface potentials are spatially uniform and event-related*, in Basar E., Bullock T.H. eds. (1989) Brain Dynamics Springer-Verlag, 158-173.
- Stein D., (1989), *Spin glasses*, Sci. Am. **July**, 36 - 42.
- Stevens C. *The Neuron*,  
in Flannagan D. ed., The Brain Scientific American Books, Freeman, ISBN 0-7167-1150-8, 15 - 25.
- Stewart I., (1989), Does God Play Dice? Basil Blackwell, Oxford.
- Stowell H., Bullock T.H., Basar E., *How brains may work : Panel discussion*,  
in Basar E., Bullock T.H. eds. Brain Dynamics, Springer-Verlag 1989, 482-511.
- Takens F., (1981), in Rand D.A., Young L.S. eds Dynamical Systems and Turbulence, Springer, Berlin.
- Tank D., Hopfield J., (1987), *Collective computation in neuron-like circuits*, Sci. Am. **Dec**, 62 - 70.
- Theiler J., (1987), *Efficient algorithm for estimating the correlation dimension from a set of discrete points*, Phys. Rev., A **36**, 4456 - 4461.
- Wintgen D., Honig A. (1989) *Irregular wave functions of a hydrogen atom in a uniform magnetic field* Phys. Rev. Lett. **63/4**, 1467-70.
- Wright J.J., (1989), *Linearity and non-linearity in electrocortical waves and their elementary statistical dynamics*, in Basar E., Bullock T.H. eds. Brain Dynamics, Springer-Verlag, 202-213.
- Wright J.J., (1990), *Reticular activation and the dynamics of neural networks*, Biol. Cybern. **62**, 289-298.
- Zhang W., Yuan J., Feng D., Pan Q., Tjon J., (1990), *Quantum fluctuations in classical chaos* Phys. Rev. A **42/6**, 3646-9.

NOTE: All diagrams are digitally processed by the author. All original sources are indicated in the text or captions.